J. Fluid Mech. (1979), *vol.* 90, *part* 4, *pp.* 725–754
Printed in Great Britain

The separating flow through a severely constricted symmetric tube

By F. T. SMITH

Department of Mathematics, Imperial College, London

(Received 14 July 1977 and in revised form 17 April 1978)

The axisymmetric flow of an incompressible fluid through a pipe (of radius a) suffering a severe constriction is studied for large Reynolds numbers R, the features of symmetric channel flows being virtually the same. Here 'severe' refers to a constriction whose typical dimensions are finite, and the oncoming velocity profile is taken to be of a realistic type, i.e. with no slip at the wall. The study adopts (Kirchhoff) free-streamline theory, which, for the mostly inviscid description, affords a rational basis consistent with viscous separation. The major (triple-deck) separation takes place on the constriction surface and is followed by a downstream eddy of length $O(aR)$. Another, less familiar, separation is predicted to occur at a distance $0{\cdot}087a \ln R + O(a)$ ahead of the finite obstacle. Free-streamline solutions are found in the two main extremes of moderately severe and very severe constriction. In both extremes, and in any slowly varying constriction, the major separation is sited near the maximum constriction point. The upstream separation point is also derived, to $O(a)$ accuracy in each case. The upstream separation can be suppressed, however, if the constriction has no definite starting point and decays slowly upstream, but then the upstream flow response extends over a much increased distance. Comparisons with Navier–Stokes solutions and with experiments tend to favour the predictions of the free-streamline theory.

1. Introduction

In the study of the incompressible fluid motion produced when a high Reynolds number (R) tube flow is symmetrically constricted, it is convenient to focus attention on constrictions of axial length comparable to the tube width or radius a. Except in extreme cases, constrictions with other axial scales provoke basically the same flow features as those with scale $O(a)$. Also, for practical applications, it is preferable to deal with incoming flows (e.g. (1.2) below) which satisfy the no-slip condition at the tube wall. We may then classify these $O(a)$ long constrictions into three basic categories, 'fine', 'moderate' and 'severe', depending on the characteristic slope α of the obstacle. For fine constrictions (Smith 1976*a*, *b*), defined by $\alpha = O(R^{-\frac{1}{3}})$, there occurs virtually no nonlinear upstream influence. A viscous nonlinear wall-layer motion is provoked adjacent to the constriction but it develops only from the start of the obstacle, not upstream, and the core motion outside the wall layer is of the inviscid elliptic, but linear, kind. Hence there is no possibility of significant nonlinear effects, such as viscous separation, ahead of the constriction. Instead any nonlinear upstream response remains suppressed, as the obstacle height is increased, until α becomes $O(R^{-\frac{1}{8}})$, which order of magnitude defines a moderate constriction. In a moderate constriction (Smith 1977*a*) the inviscid core motion is induced by the presence of the constriction

itself, rather than by the viscous wall layer near it. The pressure disturbance then feeds back, through the core, to interact nonlinearly with the wall layer upstream of the obstacle. Separation can occur, in a regular fashion, within the upstream wall layer. Further, as the obstacle height is increased on the moderate scale, the separation point is forced increasingly upstream, without bound.

The final stage in the classification process occurs when the constriction becomes severe, $\alpha = O(1)$. That is perhaps the most physically realistic case of all and is our interest in this work. Just as the moderate-constriction theory was found to be the natural development from fine-constriction theory, in the sense that these two flow structures become identical as $\alpha R^{\frac{1}{8}} \to 0$ and $\alpha R^{\frac{1}{8}} \to \infty$ respectively, so we find below that the upper limiting form of moderate-constriction theory ($\alpha R^{\frac{1}{8}} \to \infty$) indicates the basis for the severe-constriction flow structure studied here. The latter is set out in § 2 below. It is founded on classical free-streamline theory (Kirchhoff 1869), according to which no finite adverse pressure gradients can be suffered on solid surfaces (i.e. separation is smooth) and the pressure is uniform on free streamlines. The reasoning behind this approach is that free-streamline theory is believed to yield the proper inviscid limiting form of the Navier–Stokes equations, especially with regard to the viscous incompressible separation from the constriction surface. The viscous separation, which occurs in the neighbourhood of the junction between the solid surface and the downstream free streamline, is governed by triple-deck theory (Sychev 1972; Stewartson 1974; Smith 1977*b*), and part of the beauty of the triple-deck description is that it confirms the relevance of inviscid free-streamline studies.

In the present internal flow situation free-streamline theory leads in general to a problem involving nonlinear boundary conditions of mixed (free-surface and body-surface) type. The problem seems more difficult than corresponding external flow situations (e.g. Woods 1955), since a free streamline is necessary (i.e. separation occurs) far ahead of, as well as beyond, the constriction. However, on the one hand, linearization is valid if the constriction is moderately severe, and for realistic basic flows like (1.2) below, this approach produces a tractable problem (§ 3). For, unlike in external flows, the pressure on a free streamline then obeys a simple local relation with the streamline displacement. Fortunately too, at the other extreme (§ 4) where the tube is very severely constricted, so that there is only a small minimum tube width, some analytical progress is possible. In both moderate and very severe cases, and also in the slowly varying constrictions studied in § 5, the separation point on the obstacle is sited near the point of maximum constriction, a property reminiscent of the experimental observations of Föttinger (1939) and Young & Tsai (1973) (see, for example, Batchelor 1967, plate 6) and the calculations of Lee & Fung (1970) and Deshpande, Giddens & Mabon (1976). In the general case of a severe constriction (§ 2) a number of other features may be considered, including the upstream viscous separation and the ensuing slowly moving eddy, the viscous separation on the obstacle, the downstream eddy (of length $O(aR)$) and the drag on the constriction. In particular it is predicted that separation occurs asymptotically far upstream, at a distance

$$x^*_{\text{sep}} = -\tfrac{1}{8}a\beta_1^{-1}\ln R + (0{\cdot}566 - \ln\overline{\pi}_1)\beta_1^{-1}a + o(a) \tag{1.1}$$

ahead of the constriction. Here $\beta_1 = 3{\cdot}83$, $\overline{\pi}_1$ is a constant to be calculated from free-streamline theory (see, for example, §§ 3 and 5) and R is defined precisely below. The result (1.1) holds for axisymmetric pipe flow, upon which we concentrate mainly

hereafter. Symmetric channel flows have essentially the same characteristics. Asymmetric channels and pipes provoke very different features, however (Smith 1976*b*, *c*, 1977*c*), as do dilatations (Smith 1976*a*, *b*).

The result (1.1) does not hold, however, if the constriction has no definite starting point and decays slowly (e.g. algebraically) upstream. Then the upstream separation does not occur, but a very long scale upstream adjustment is provoked (§ 6).

Comparisons with experiments and with Navier–Stokes solutions, presented in the appendix, encourage the belief in the relevance of free-streamline theory at high Reynolds numbers.

The Reynolds number is defined by $R = U_\infty a/\nu\,(\gg 1)$, where U_∞ is twice the maximum velocity of the flow far upstream of the constriction, the tube being straight apart from the constriction. The fluid is incompressible with kinematic viscosity ν and density ρ and its motion is assumed to remain laminar, steady and symmetric throughout. As incoming profile, sufficiently far upstream, for convenience we take Poiseuille flow

$$u = U_0(r) \equiv \tfrac{1}{2}(1-r^2), \quad \psi = \Psi_0(r) \equiv -\tfrac{1}{8}(1-r^2)^2, \quad v = 0, \quad \partial p/\partial x = -2/R, \tag{1.2}$$

although the theory applies to more general (e.g. undeveloped) forms. Here u, v, ψ, p, x and r denote the axial and radial velocities, stream function ($u = \partial\psi/r\,\partial r, v = -\partial\psi/r\,\partial x$), pressure and axial and radial co-ordinates, non-dimensionalized with respect to U_∞, U_∞, a^2U_∞, ρU_∞^2, a and a in turn. The (smooth) constriction is prescribed by

$$r = 1 - F(x), \tag{1.3}$$

where $F(x)$ is zero upstream of the constriction and has a maximum $F_{\max}(<1)$ at $x = x_{\max}$, say.

The study here has clear relevance to many engineering problems (e.g. oil pipelines or machinery dynamics), to physiological flows, to wall interference in wind-tunnel testing (see, for example, Grove *et al.* 1964) and, possibly, to the performance of certain musical instruments. Work has been done on similar themes (e.g. Sobey 1976; Fraenkel 1961; Yih 1959, 1960) although often (for various reasons) by use of physical models and/or integral methods that perhaps tend to obscure some of the important flow details, and with unrealistic incoming profiles.

2. Symmetric constrictions of finite length (or semi-infinite)

The approach we adopt here for the flow through a severe constriction is based on an extension of Kirchhoff's (1869) free-streamline theory (with smooth separation), which has been shown (Sychev 1972; Smith 1977*b*) to provide a rational basis for the description of high Reynolds number flow past bluff bodies in external flows. Thus we are led to seek a solution of the inviscid equations of motion in which on any solid surfaces only favourable finite pressure gradients are permitted (to avoid a catastrophe at separation; Stewartson 1970*a*, 1974; Goldstein 1948), while on any free streamlines the pressure is to be uniform (so that no sizable reversed flow is generated between the tube wall and the shear layer surrounding the free streamline). Clearly, for a finite body, these demands require breakaway (and, consequently, boundary-layer separation) of the motion before it reaches the rear of the body. Otherwise, an adverse pressure gradient is provoked as the fluid slows down near the rear. But, less familiarly,

breakaway and separation must occur upstream as well, to avoid the adverse pressure gradient that would otherwise arise during the deceleration at the wall near the front of the constriction. Further, the position of this upstream separation point may be shown to be asymptotically far upstream when $R \gg 1$ (see below), so that the inviscid solution holding at finite distances from the constriction begins with a separation streamline upstream. We return to discuss the upstream separation below. For the motion in the core, where x and r are $O(1)$ (apart from in the zones of reversed motion and in the thin viscous layers), we have

$$(\psi, u, p) = (\psi_0, u_0, p_0) + R^{-M}(\psi_1, u_1, p_1) + o(R^{-M}), \tag{2.1}$$

where the index M (> 0) is referred to below. Hence ψ_0, u_0 and p_0 satisfy the inviscid equations of motion, which yield, on integration and use of the starting condition (1.2), the vorticity equation

$$D^2\psi_0 = -r^2, \tag{2.2}$$

where $D^2 = (\partial^2/\partial r^2 - r^{-1}\partial/\partial r + \partial^2/\partial x^2)$. The boundary conditions on the inviscid solution are

$$\psi_0 = 0 \quad \text{on the body or free streamlines,} \tag{2.3a}$$

$$p_0 \text{ uniform on free streamlines,} \tag{2.3b}$$

$$\psi_0 = -\tfrac{1}{8} \quad \text{at} \quad r = 0 \quad \text{(for symmetry),} \tag{2.3c}$$

$$\psi_0(-\infty, r) = \Psi_0(r) \quad \text{[from (1.2)]} \tag{2.3d}$$

(see also (2.10) below). In fact (2.3b) may be made more specific for the upstream and downstream portions of the free streamline (figure 1). The arbitrary upstream pressure constant may be chosen to be zero, so, since Bernoulli's equation holds,

$$p_0 = 0 \quad (u_0 = 0) \quad \text{on the free streamline } C_0C_1, \tag{2.4a}$$

$$p_0 = p_{00} \quad [u_0 = (-2p_{00})^{\frac{1}{2}}] \quad \text{on the free streamline } C_2C_3. \tag{2.4b}$$

Here the constant p_{00} is negative because the pressure falls along the constriction C_1C_2 (and an attached boundary layer of thickness $O(R^{-\frac{1}{2}})$ is produced along C_1C_2). The pressure p_0 and its gradient $\partial p_0/\partial x$ are required to be continuous at C_2 (for smooth separation), which condition fixes the solution for ψ_0.

The breakaway point C_2 (where $x = x_2 + R^{-M}x_{21} + o(R^{-M})$) and the reattachment point C_1 ($x = x_1 + O(R^{-M})$) upstream of it have to be determined, as do the shapes of the free streamlines C_0C_1 (where $1 - r = F_1(x) + O(R^{-M})$) and C_2C_3 (where

$$1 - r = F_2(x) + R^{-M}F_{21}(x) + o(R^{-M})).$$

However, we may verify that the first separation point C_0 is asymptotically far upstream, as follows. For $x \to -\infty$ the solution of (2.2) must take the form

$$\psi_0 \sim \Psi_0(r) - \pi_1 \exp(\beta_1 x)\frac{rJ_1(\beta_1 r)}{\beta_1 J_1'(\beta_1)} + O(\exp(\beta_2 x)), \tag{2.5}$$

where π_1 is an unknown constant (see, for example, § 3 below) and β_n is the nth positive zero of the first-order Bessel function J_1. Since, on physical grounds, the fluid must accelerate along the centre-line in anticipation of the coming constriction, we may assume that $\pi_1 > 0$. Then the velocity is

$$u_0 \sim U_0(r) - \frac{\pi_1 \exp(\beta_1 x)}{J_1'(\beta_1)}J_0(\beta_1 r) + O(\exp(\beta_2 x)) \tag{2.6a}$$

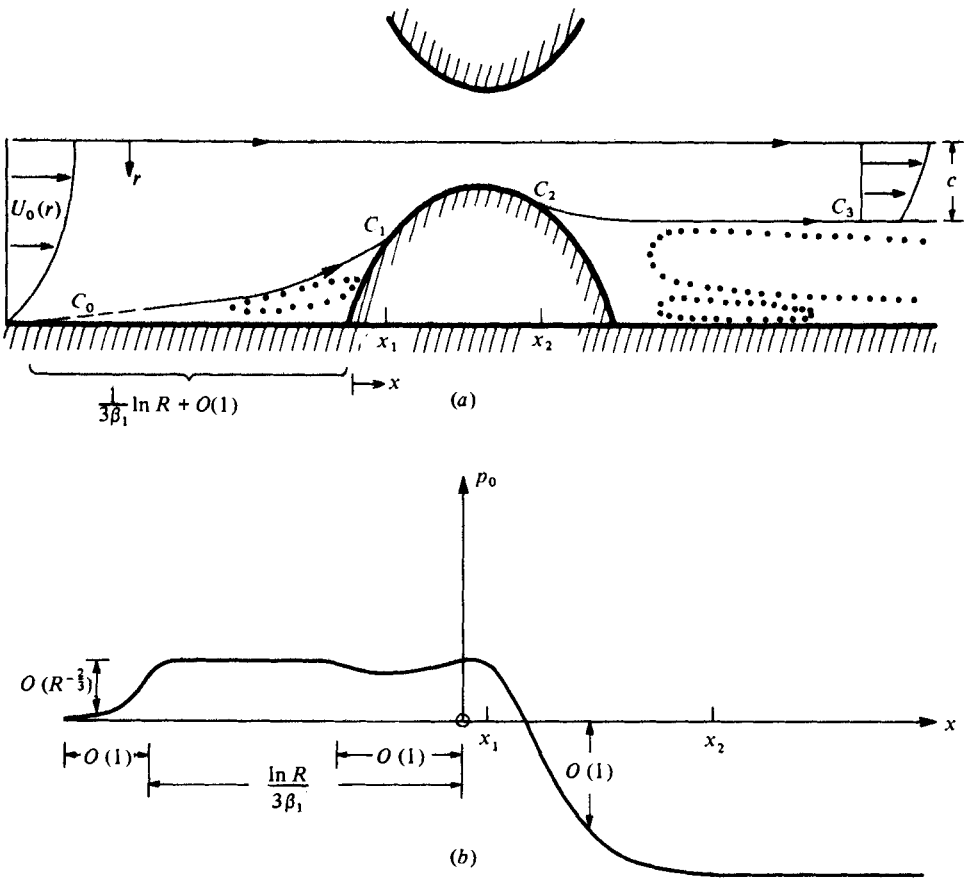

FIGURE 1. (*a*) The severely constricted tube flow field and definitions. The main, free-streamline motion is shown by solid lines, the slower eddying motions by dotted lines. (*b*) Sketch (not to scale) of the wall pressure variation through the tube.

for $x \to -\infty$ (here J_0 is the zeroth-order Bessel function). If the flow were attached to the wall here then the slip velocity driving the viscous wall layer would be given by the value of (2.6*a*) at $r = 1$, which is negative. Not surprisingly, the corresponding Falkner–Skan problem in the wall layer has no solution. The resolution of this contradiction is that the flow has already separated and there exists a free streamline (a line of discontinuity) at $1 - r = F_1(x)$ (in $x < x_1$) with the property

$$F_1(x) \sim \pi_1 \exp(\beta_1 x) \quad \text{for} \quad x \to -\infty, \tag{2.6b}$$

to conform with the uniform-pressure requirement (2.4*a*). This result matches with the results for moderate constrictions (Smith 1977*a*) and demonstrates the invalidity of continuous inviscid theory (Sobey 1976; Fraenkel 1961; Yih 1959, 1960) for realistic incoming profiles like (1.2).

The viscous separation far upstream, near C_0, occurs in a viscous wall zone, whose thickness is $O(R^{-\frac{1}{3}})$ for the balance of inertial and viscous forces. The basic flow (1.2) has velocity $O(R^{-\frac{1}{3}})$ in such a layer, so it is perturbed nonlinearly when the slip velocity (at $r = 1-$) induced by (2.6*a*) also becomes $O(R^{-\frac{1}{3}})$. This takes place when $\exp(\beta_1 x)$

[in (2.6a)] is $O(R^{-\frac{1}{8}})$. We set $x = -\frac{1}{3}\beta^{-1}\ln R + \bar{x}$, therefore, where $\bar{x}$ is $O(1)$, so that x is large and negative. Then the flow structure for $\bar{x} = O(1)$ is mainly an inviscid core (i) wherein $\psi = \Psi_0(r) + R^{-\frac{1}{8}}\overline{\psi}_1(\bar{x}, r) + \ldots$, and

$$\overline{\psi}_1(\bar{x}, r) = -\pi_1 \exp(\beta_1 \bar{x}) \frac{rJ_1(\beta_1 r)}{\beta_1 J_1'(\beta_1)} \quad \text{for all } \bar{x}. \tag{2.6c}$$

The other eigensolutions for $\overline{\psi}_1$ (which satisfies $D^2\overline{\psi}_1 = 0$) are proportional to $\exp(\beta_n \bar{x})$ with $n \geqslant 2$ and consequently are inadmissible because they grow too fast to match with (2.5) when $\bar{x} \to +\infty$ [and $x \to -\infty$ in (2.5)]. [If π_1 were zero then the $\exp(\beta_2 \bar{x})$ term would be appropriate; the basic properties of the upstream separation are unaltered in this special case, however.] A wall zone (ii) reduces the $O(R^{-\frac{1}{8}})$ slip velocity associated with (2.6c) to zero. In (ii), $u = R^{-\frac{1}{8}}\overline{U}(\bar{x}, Z)$ and $\psi = -R^{-\frac{3}{8}}\overline{\Psi}(\bar{x}, Z)$, where $r = 1 - R^{-\frac{1}{8}}Z$ and Z is $O(1)$, and $\overline{U}$ and $\overline{\Psi}$ satisfy the boundary-layer equations

$$\overline{U} = \frac{\partial \overline{\Psi}}{\partial Z}, \quad \overline{U}\frac{\partial \overline{U}}{\partial \bar{x}} - \frac{\partial \overline{\Psi}}{\partial \bar{x}}\frac{\partial \overline{U}}{\partial Z} = -\frac{d\overline{P}}{d\bar{x}} + \frac{\partial^2 \overline{U}}{\partial Z^2}. \tag{2.7a}$$

Here $\overline{P}(\bar{x}) \equiv R^{\frac{3}{8}}p$ and is one of the unknowns in (ii). The boundary conditions on $\overline{U}$ and $\overline{\Psi}$ are

$$\overline{U} = \overline{\Psi} = 0 \quad \text{at} \quad Z = 0, \tag{2.7b}$$

$$\overline{U} \to Z, \quad \overline{\Psi} \to \tfrac{1}{2}Z^2, \quad \overline{P} \to 0 \quad \text{as} \quad \bar{x} \to -\infty, \tag{2.7c}$$

$$\overline{U} \sim Z - \pi_1 \exp(\beta_1 \bar{x}) \quad \text{as} \quad Z \to \infty. \tag{2.7d}$$

The constraints (2.7b–d) ensure, respectively, the no-slip condition, the match with the Poiseuille flow (1.2) upstream and the join to the core (i) [since the slip velocity from (2.6c) is $-\pi_1 R^{-\frac{1}{8}} \exp(\beta_1 \bar{x})$]. The solution of (2.7$a$–$d$) has been calculated by Smith (1977a). The wall zone separates at a finite value $\bar{x}_{\text{sep}}$ of $\bar{x}$, given by

$$\bar{x}_{\text{sep}} = 0{\cdot}566\beta_1^{-1} - \ln(\overline{\pi}_1)/\beta_1 \quad (\overline{\pi}_1 = \beta_1^{\frac{1}{8}}\pi_1).$$

Thereafter the fluid in the wall zone starts to concentrate in a shear layer centred around the curve

$$Z = \pi_1 \exp(\beta_1 \bar{x}). \tag{2.8a}$$

As $\bar{x} \to +\infty$ the solution generates the following self-similar structure. First, surrounding the curve (2.8a) there is the shear layer of thickness $O(\bar{x}^{\frac{1}{2}})$ in which

$$\overline{U} = \bar{x}^{\frac{1}{2}}G_0'(\xi), \quad \overline{\Psi} = \bar{x}^{\frac{3}{2}}G_0(\xi), \tag{2.8b}$$

where $\xi = [Z - \pi_1 \exp(\beta_1 \bar{x})]\bar{x}^{-\frac{1}{2}}$, and $G_0(\xi)$ has the property $G_0(-\infty) = -C_0 (= -1{\cdot}2521$; see Stewartson & Williams 1973). Second, there is a viscous sublayer near the wall, of thickness $O(\bar{x}^{\frac{1}{2}} \exp(-\beta_1 \bar{x}))$. Between the two layers a slow, reversed, uniform streaming preserves the mass entrainment required by (2.8b). Hence, as the flow emerges downstream ($\bar{x} \to +\infty$) from the separation zone (ii), the dividing streamline takes up the position $r \sim 1 - \pi_1 R^{-\frac{1}{8}} \exp(\beta_1 \bar{x})$, from (2.8$a$). This position continues directly into (2.6b) (where $x \to -\infty$). Also, an overall pressure rise $R^{-\frac{3}{8}}\overline{P}(\infty)$, where $\overline{P}(\infty) = 0{\cdot}95$, is produced through the separation zone (ii). Finally, the upstream separation point is predicted to be at $x = x_{\text{sep}}$, where

$$x_{\text{sep}} = -\tfrac{1}{3}\beta_1^{-1}\ln R + (0{\cdot}566 - \ln \overline{\pi}_1)\beta_1^{-1} + o(1). \tag{2.9}$$

The value of $\overline{\pi}_1$, which depends on the whole motion for $x = O(1)$, is therefore one of the principal unknowns (see, for example, (3.19) and (5.10) below).

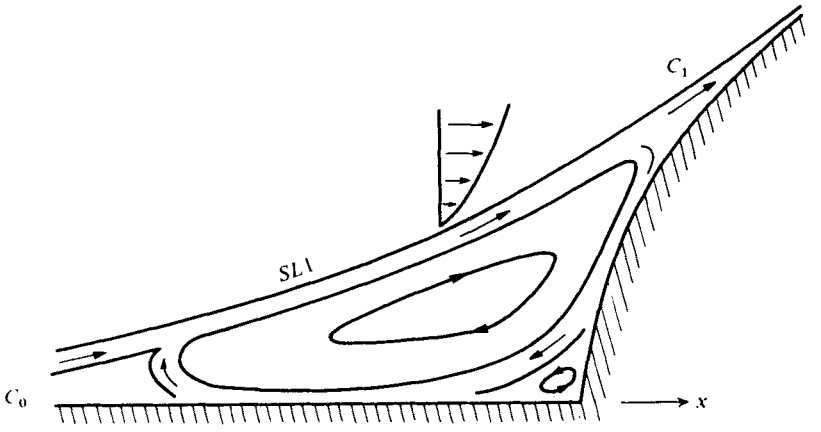

FIGURE 2. Diagram of the upstream eddy and shear layer ($SL1$).

If the constriction shape [see (1.3)] has $F(x) = 0$ for $x < 0$, say, then a numerical solution of the basic problem (2.2)–(2.4) (with (2.10) below) would seem necessary when F is generally $O(1)$ (see however § 5). The conformal mapping methods applicable in a limited number of exterior flow problems (e.g. Milne-Thompson 1968; Batchelor 1967) do not usually yield a viable calculation technique here. Before considering (in §§ 3–5) certain limiting solutions of the basic problem, however, we may anticipate some other important features of the overall motion.

First, near $x = x_2$, $p_0 - p_{00} \propto (x_2 - x)^{\frac{3}{2}}$ as $x \to x_2-$ (while $p_0 = p_{00}$ for $x > x_2$) and $F_2(x_2) - F_2(x) \propto (x - x_2)^2 + O(x - x_2)^{\frac{5}{2}}$ as $x \to x_2+$, since in the neighbourhood of $x = x_2$, (2.2) gives potential flow to first order. This necessary (smooth separation) property of the free-streamline theory is in line with the triple-deck description of incompressible separation Smith (1977*b*), occurring at $x = x_2 + O(R^{-\frac{3}{8}})$, provided that $M = \frac{1}{16}$ (Sychev 1972) in (2.1) and $p_1 - p_{10} \propto (x_2 - x)^{\frac{1}{2}}$ as $x \to x_2-$, while $F_{21} \propto (x - x_2)^{\frac{3}{2}}$ for $x \to x_2+$. Here p_{10} is the uniform value of p_1 on the free streamline C_2C_3 and the values of the constants of proportionality in $p_1 - p_{10}$ and F_{21} above are given numerically by Smith (1977*b*).

Next we consider briefly the eddying motion between C_0C_1 and the wall, and the reattachment at C_1, sketched in figure 2. Both are necessary to maintain the mass flux required by the thin shear layer ($SL1$) around C_0C_1. The structure of eddies and reattachment in general is by no means clear yet (Burggraf 1970, 1975; Messiter, Hough & Feo 1973; Jenson, Burggraf & Rizzetta 1974), however, and only the following, essentially qualitative (or order-of-magnitude), remarks are appropriate. The solution in $SL1$ starts as the continuation of (2.8*b*), so that the typical velocities in $SL1$ are $O(\delta = (R^{-1} \ln R)^{\frac{1}{3}})$ when x is finite, and a mass flux $O(\delta^2)$ (entrained by $SL1$) needs to be reversed, ahead of C_1, to preserve continuity. A pressure variation of order δ^2 is required for this purpose, from Bernoulli's law. In some related problems Burggraf (1975), Jenson *et al.* (1974), Smith & Duck (1977) and Professor K. Stewartson (1977, private communication) have proposed that reattachment exhibits locally a sharp pressure rise ($O(\delta^2)$ here) and source-like behaviour which sustain an entraining motion in the eddy. Conversely, the approach of Burggraf (1970) and Messiter *et al.* (1973), while suggesting the sharp $O(\delta^2)$ pressure rise close to reattachment, in order to

turn back the negative mass flux remaining in $SL1$ at $x = x_1-$, results in a backward wall jet [with velocity $O(\delta)$] emerging from the neighbourhood of C_1. Further away from C_1, on the length scale $x = O(1)$, the effects of the backward jet and the shear layer $SL1$ then combine to produce an essentially inviscid eddy, of closed streamlines, in which the velocity and pressures are again $O(\delta)$ and $O(\delta^2)$ in turn. This eddy, which rotates clockwise, is of the Prandtl–Batchelor type (Batchelor 1956), with constant vorticity. But since it lies between C_0C_1 and the wall, and C_0C_1 is fixed from (2.2)–(2.4), there is no interaction between the eddy pressure $[O(\delta^2)]$ and its shape, unlike in the Messiter *et al.* (1973) model. We tend to favour the Burggraf (1970) and Messiter *et al.* (1973) approach, despite the difference mentioned above, but note that there is a distinct possibility that, following the interaction (along C_0C_1) between the eddy slip velocity and the shear-layer velocity, the $SL1$ profile entering the reattachment zone around C_1 contains no negative mass flux. In that case the reattachment process near C_1 is a relatively passive process, involving no sharp pressure rise. In either event, however, a secondary separation seems inevitable as the fluid in the wall layer decelerates on approaching the discontinuity at the onset of constriction ($x \to 0+$).

Another property is the relation between the drag C_D (or axial force) acting on the constriction and the ultimate form of the inviscid solution far downstream as $x \to +\infty$. The only ultimate form consistent with (2.2), (2.3*a*, *c*) and (2.4*b*) seems to be a jet-like inviscid motion, bounded by lines of constant radius ($r = c$; figure 1). Thus

$$\left.\begin{aligned} &F_2(x) \to 1-c, \quad p = p_{00}, \\ &u_0 \to -\tfrac{1}{2}r^2 + \tfrac{1}{4}(c^2+c^{-2}), \\ &\psi_0 \to -\tfrac{1}{8}[1+r^4-(c^2+c^{-2})r^2] \end{aligned}\right\} \quad \text{for} \quad x \to +\infty. \tag{2.10}$$

The constants c ($0 < c < 1$) and p_{00} here are related by the condition

$$-p_{00} = \tfrac{1}{32}(c^{-4}-2+c^4),$$

from Bernoulli's theorem. In addition, however, an integral momentum balance (taking into account the uniform surface pressures $p_0 = 0$ and $p_0 = p_{00}$ upstream of C_1 and downstream of C_2 respectively) yields the formula

$$C_D = (\pi/96c^4)(1-c^2)^3(3+3c^2+2c^4). \tag{2.11}$$

Hence C_D is $O(1)$ and positive, provided $c < 1$, i.e. if separation takes place. Figure 3 details the dependence of the drag C_D and free-streamline pressure p_{00} on the final jet radius c. Both C_D and $-p_{00}$ increase (from zero) relatively slowly as c falls from unity to about 0·4, but they rise rapidly as c decreases further.

Lastly, far downstream the flow must reattach to provide the small mass flux which is entrained by the $O(R^{-\frac{1}{2}})$ shear layer surrounding C_2C_3. The reattachment occurs at a distance $O(R)$ beyond the constriction. (See, for example, Deshpande *et al.* 1976, figures 5*a*, *b*; Lee & Fung 1970). This is because the shear-layer solution is, for $x \gg 1$, $\psi \sim R^{-\frac{1}{2}}x^{\frac{1}{2}}\mathscr{F}(\eta)$ (where $\mathscr{F}$ is a similarity function (e.g. Lock 1951) and $\eta = (r-c)R^{\frac{1}{2}}x^{-\frac{1}{2}}$), so that when x is $O(R)$ the shear layer becomes of thickness $O(1)$, comparable with the pipe width. At that stage the part of the fluid moving with velocity $O(1)$ must expand to fill the tube, inducing reattachment. This reattachment process and some others (e.g. Hung & Macagno 1966; Macagno & Hung 1967; Lee & Fung 1970) are currently being studied. In particular, it is likely that the slower reversed motion between

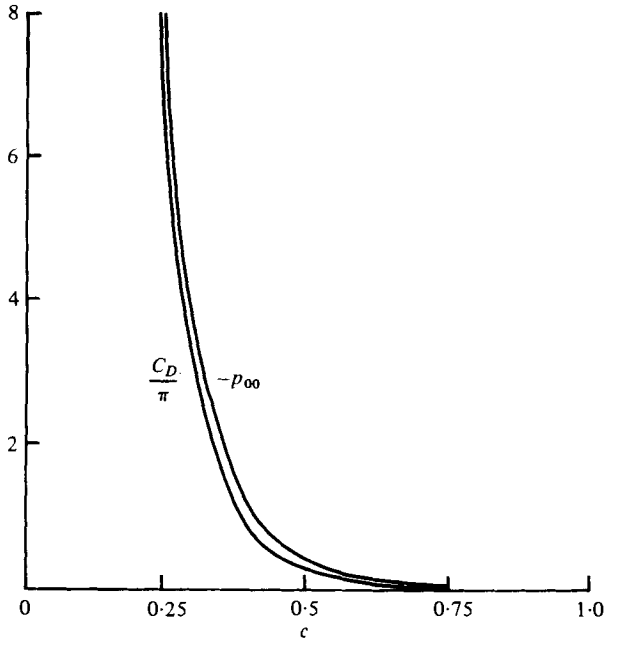

FIGURE 3. Graphs of C_D and p_{00} against c [see (2.10) and (2.11)].

C_2C_3 and the wall contains not one but *two* secondary eddies, both of axial length $O(R)$ and radial extent $O(1)$. This occurrence is like that within the upstream eddy, and is due essentially to an adverse pressure gradient which is induced as the reversed flow decelerates on approaching from far downstream.

The description of all the eddies, separations, reattachments and other details depends on the solution of the central problem (2.2)–(2.4) [with (2.10)], which is attempted in §§ 3–5 below for moderately severe, very severe and slowly varying severe constrictions respectively.

3. Moderately severe constrictions

We may progress analytically if we make the assumption $|F| \ll 1$ now, so that the wall is only slightly perturbed (but still on the severe scale). Let us suppose that $F = h\bar{F}(x)$, where $|\bar{F}|$ is $O(1)$ but $h \ll 1$. Then formally the solution of (2.2) may be linearized about the initial profile (1.2) in the form

$$\left.\begin{aligned} \psi_0 &= \Psi_0(r) + h^2\psi_{01} + h^3\psi_{02} + \ldots, \\ u_0 &= U_0(r) + h^2u_{01} + h^3u_{02} + \ldots, \\ p_0 &= h^2p_{01} + h^3p_{02} + \ldots, \end{aligned}\right\} \tag{3.1}$$

where, from (2.2),

$$D^2\psi_{01} = 0 = D^2\psi_{02} = \ldots. \tag{3.2}$$

The fact that the $O(h)$ wall disturbance provokes only $O(h^2)$ flow perturbations of (1.2) is due entirely to the no-slip property of the basic motion (1.2). The boundary conditions on ψ_{01}, ψ_{02}, etc. are obtained by expanding

$$F_2 = hf_{20}(x) + h^2f_{21}(x) + h^3f_{22}(x) + O(h^4), \quad F_1 = hf_{10}(x) + h^2f_{11}(x) + h^3f_{12}(x) + O(h^4)$$

for the constraints (2.3) and using the definitions

$$U(x) = hf_{i0} + h^2[u_{01}(x,1) + f_{i1} - \tfrac{1}{2}f_{i0}^2] + h^3[u_{02}(x,1) + f_{i2} - f_{i0}f_{i1} - f_{i0}\,\partial u_{01}(x,1)/\partial r] + O(h^4) \tag{3.3}$$

for the slip velocity $U(x)$ along the free streamlines C_0C_1 (on which $i = 1$) and C_2C_3 ($i = 2$), respectively. Since $U(x)$ must be zero on C_0C_1, we have (from (3.3) with $i = 1$)

$$f_{10}(x) \equiv 0, \quad f_{11}(x) = -u_{01}(x,1), \quad f_{12}(x) = -u_{02}(x,1) \tag{3.4a}$$

(and $u_{01}(x,1)$ is negative in $x < 0$ for any constriction $\bar{F}$; see (3.17a) below). The conditions (3.5a) and (3.6a) below then follow. Hence the upstream free streamline is much closer [distance $O(h^2)$] to the wall than is the downstream one [distance $O(h)$, from (3.4b) below). Also the result (assumed in (3.5a) below) that $x_1 \ll 1$ stems from (3.4a) (see more precise evaluation of x_1 below). Again, (2.4) and (3.3) imply that $f_{20}(x)$ is uniform, that $x_2 = x_{\max}[+o(1)]$ (see (3.11) below) and hence that

$$f_{20}(x) \equiv \bar{F}(x_{\max}), \quad f_{21}(x) = u_{01}(x_{\max}+,1) - u_{01}(x,1) \tag{3.4b}$$

(see note below on the effect of $f_{21}(x)$ on the shear-layer shape C_2C_3), where the result for $f_{21}(x)$ holds for $x > x_2$ and x_2 is determined in (3.13) below. From (3.4a, b) and Taylor series expansions in (2.3) the boundary conditions on ψ_{01} and ψ_{02} become

$$\psi_{01}(x,1-) = \begin{cases} 0 \quad \text{for} \quad x < 0, & (3.5a) \\ \tfrac{1}{2}\bar{F}^2 \quad \text{on the constriction, for} \quad 0 < x < x_{\max}, & (3.5b) \\ \tfrac{1}{2}f_{20}^2 \quad \text{on the downstream free streamline, for} \quad x > x_{\max}, & (3.5c) \end{cases}$$

$$\psi_{02}(x,1-) = \begin{cases} 0 \quad \text{for} \quad x < x_1, & (3.6a) \\ -\tfrac{1}{2}\bar{F}^3 + \bar{F}u_{01}(x,1) \quad \text{on the constriction}, & (3.6b) \\ -\tfrac{1}{2}f_{20}(f_{20}^2 - 2f_{21}) + f_{20}\,u_{01}(x,1) \quad \text{for} \quad x > x_2. & (3.6c) \end{cases}$$

Before giving the global solution for ψ_{01} (in (3.13)–(3.17) below) we may deduce a number of the linearized flow properties. First, the precise value of x_1 when h is small depends strongly on the particular shape of the constriction, for the criterion for determining x_1 is that $U(x_1+) = 0$, where

$$U(x) = h\bar{F}(x) + h^2[-\tfrac{1}{2}\bar{F}^2(x) + u_{01}(x,1)] + h^3[-\bar{F}(x)\,\partial u_{01}(x,1)/\partial r + u_{02}(x,1)] + O(h^4) \tag{3.7}$$

gives the slip velocity on the body, $x_1 < x < x_2$. Therefore we need the behaviour of u_{01} in particular as $x \to 0+$ [since $x_1 \ll 1$ from (3.4a)]. This comes from a local examination of ψ_{01} near $x = 0$. If, say, the constriction is wedge-like at its start, so that $\bar{F}(x) = K_0x + K_1x^2 + O(x^3)$ for $x \to 0+$, where K_0 and K_1 are constants with $K_0 > 0$, and $\bar{F}(x) = 0$ for $x < 0$, then (3.2) and (3.5a, b) yield the property

$$\psi_{01} \sim d_1\hat{r}_1\sin\theta - \frac{K_0^2\hat{r}_1^2}{2\pi}[(\theta-\pi)\cos 2\theta + (\ln\hat{r}_1)\sin 2\theta] + d_2\hat{r}_1^2\sin^2\theta \tag{3.8}$$

for $\hat{r}_1 \ll 1$, where $\hat{r}_1^2 = x^2 + (1-r)^2$, $0 < \theta = \tan^{-1}(\hat{r}_1/x) \leqslant \pi$, and d_1 and d_2 are constants. Therefore $u_{01}(0,1)$ is finite (and negative, from (3.17a) below) but

$$u_{01}(x,1) - u_{01}(0,1) \sim \pm(K_0^2/\pi)\,|x|\ln|x| \quad \text{as} \quad x \to 0\pm.$$

With (3.7) this suggests the expansion

$$x_1 = hx_1^{(1)} + h^2 \ln hx_1^{(2)} + O(h^2 \ln(-\ln h)) \tag{3.9a}$$

for x_1. Substituting into the constraint $U(x_1) = 0$ and using Taylor series, we find

$$x_1^{(1)} = -u_{01}(0,1)/K_0, \quad x_1^{(2)} = u_{01}(0,1)/\pi. \tag{3.9b}$$

(A referee has kindly pointed out that the value for $x_1^{(1)}$ in (3.9*b*) follows more directly as the intersection of the free streamline (3.4*a*) with the constriction surface. The same applies to the first term in (3.10) below.) By contrast, if the constriction is bluff near its start, with $\bar{F} \sim K_0 x^N$ for $0 < x \ll 1$, where $K_0 > 0$ and $\frac{1}{2} < N < 1$, then an analysis similar to (3.8)–(3.9) yields the expansion

$$x_1 = -h^{1/N} u_{01}(0,1)/K_0 - h^2 K_0^{1-N}(-u_{01}(0,1))^N \cot(2N\pi) + \ldots. \tag{3.10}$$

[If $N = \frac{1}{2}$, log terms again appear in the expansion of ψ_{01} but (unlike in (3.10)) the linearization of (3.1) then becomes invalid (or indeed if $N < \frac{1}{2}$) around the reattachment point.] Hence, as N decreases, the reattachment point moves further upstream, towards the onset of constriction, because the increased bluffness of the constriction promotes more rapidly the acceleration necessary to maintain a forward-moving wall layer beyond reattachment.

Second, the separation point x_2 is less dependent on the constriction shape when $h \ll 1$; in general it is described by

$$x_2 = x_{\max} + h \ln hx_2^{(1)} + O(h \ln(-\ln h)). \tag{3.11a}$$

Substitution of (3.11*a*) into the constraint $dU(x = x_2-)/dx = 0$ for smooth separation (Sychev 1972; Smith 1977*b*), with $U(x)$ prescribed by (3.7), together with a local analysis like (3.8) and (3.9), yields

$$x_2^{(1)} = \pi^{-1} \bar{F}_{\max}. \tag{3.11b}$$

Hence the separation point is just upstream of the maximum constriction point, regardless of the particular shape $\bar{F}(x)$ provided that $\bar{F}$ is smooth. This property compares with separation positions in external free-streamline flows, the latter also tending to separate over the forward face of an obstacle (see, for example, Brodetsky 1923) but well before the position of maximum obstruction.

Third, the drag C_D on the obstacle becomes

$$C_D \approx \tfrac{2}{3}\pi h^3 \bar{F}_{\max}^3 + O(h^4) \tag{3.12}$$

when h is small, since here $c \to 1 - h\bar{F}_{\max}$ in (2.11).

The general solution for ψ_{01} in $x < 0$ is, from (3.2) and (3.5),

$$\psi_{01} = -r \sum_{n=1}^{\infty} \frac{\hat{\gamma}_{0n} J_1(\beta_n r)}{J_1'(\beta_n)} \exp(\beta_n x), \tag{3.13}$$

where $$0 < 2\hat{\gamma}_{0n} = \int_0^{x_{\max}} \bar{F}^2(\xi) \exp(-\beta_n \xi)\, d\xi + \frac{\bar{F}_{\max}^2}{\beta_1} \exp(-\beta_n x_{\max}).$$

The general solution may also be written down formally for $x > 0$† but it is more useful to take a specific case. If we choose the parabolic-shaped constriction (Smith 1977*a*)

$$2\tfrac{1}{2}F(x) = hx(2L-x)L^{-2} \quad \text{for} \quad 0 < x < 2L \tag{3.14}$$

then separation occurs at $x = x_{\max} = L$, so that $f_{20} = 2^{-\frac{1}{2}}$ for $x > L$, from (3.4*b*). Then ψ_{01} is given by

$$\psi_{01} = G(x,r) - \sum_{n=1}^{\infty} \frac{rJ_1(\beta_n r)}{L^2 J_1'(\beta_n)} \exp(\beta_n \hat{x})(\beta_n^{-3} - 6L^{-2}\beta_n^{-5}) \tag{3.15}$$

for $0 < x < L$ and by

$$\psi_{01} = G(x,r) + \sum_{n=1}^{\infty} \frac{rJ_1(\beta_n r)}{L^2 J_1'(\beta_n)} (\beta_n^{-3} - 6L^{-2}\beta_n^{-5}) \exp(-\beta_n \hat{x})$$
$$- \frac{r^2}{L^2}\left[\frac{6}{L^2}\left\{\left(\frac{1-r^2}{64}\right) + \left(\frac{r^4-1}{192}\right) + \left(\frac{1-r^2}{16}\right)\hat{x}^2 + \frac{\hat{x}^4}{24}\right\} + \left\{\left(\frac{r^2-1}{8}\right) - \frac{\hat{x}^2}{2}\right\}\right] \tag{3.16}$$

for $x > L$. Here $\hat{x} = x - L$ and

$$G(x,r) = 2\sum_{n=1}^{\infty} \frac{rJ_1(\beta_n r)}{L^2 J_1'(\beta_n)} \exp(-\beta_n x)\beta_n^{-3}\left(1 + \frac{3}{\beta_n L} + \frac{3}{\beta_n^2 L^2}\right) + \frac{2r^2}{L^2}\left[\frac{3}{L^2}\left\{\left(\frac{1-r^2}{64}\right)\right.\right.$$
$$\left.\left. + \left(\frac{r^4-1}{192}\right) + \left(\frac{1-r^2}{16}\right)x^2 + \frac{x^4}{24}\right\} - \frac{3}{L}\left\{\left(\frac{1-r^2}{8}\right)x + \frac{x^3}{6}\right\} + \left\{\frac{x^2}{2} + \left(\frac{1-r^2}{8}\right)\right\}\right].$$

For this example we have also

$$u_{01}(x,1) = -\sum_{n=1}^{\infty} \beta_n \bar{\gamma}_{0n} \exp(\beta_n x) \quad \text{for} \quad x < 0, \tag{3.17a}$$

$$u_{01}(x,1) = -\sum_{n=1}^{\infty} \exp(\beta_n \hat{x}) \frac{\beta_n}{L^2}(\beta_n^{-3} - 6L^{-2}\beta_n^{-5}) + 2\sum_{n=1}^{\infty} \frac{\exp(-\beta_n x)}{L^2 \beta_n^2}$$
$$\times \left(1 + \frac{3}{\beta_n L} + \frac{3}{\beta_n^2 L^2}\right) + \left[L^{-4}\left(\frac{x^4}{2} - \frac{1}{16} - \frac{3x^2}{4}\right) + L^{-3}\left(\frac{3x}{2} - 2x^3\right)\right.$$
$$\left. + L^{-2}(2x^2 - \tfrac{1}{2})\right] \quad \text{for} \quad 0 < x < L, \tag{3.17b}$$

and

$$u_{01}(x,1) = -\sum_{n=1}^{\infty} \exp(-\beta_n \hat{x}) \frac{\beta_n}{L^2}\left(\frac{6}{L^2\beta_n^5} - \frac{1}{\beta_n^3}\right) + 2\sum_{n=1}^{\infty} \frac{\exp(-\beta_n x)}{L^2 \beta_n^2}$$
$$\times \left(1 + \frac{3}{\beta_n L} + \frac{3}{\beta_n^2 L^2}\right) + \left[L^{-4}\left(\frac{x^4}{2} - \frac{\hat{x}^4}{2} - \tfrac{3}{4}x^2 + \tfrac{3}{4}\hat{x}^2\right) + L^{-3}\left(\frac{3x}{2} - 2x^3\right)\right.$$
$$\left. + L^{-2}(2x^2 + \hat{x}^2 - \tfrac{3}{4})\right] \quad \text{for} \quad x > L. \tag{3.17c}$$

† The Fourier transform of (3.2), with $\psi_{01}(x,0) = 0$, yields the formal solution

$$\psi_{01}(x,r) = \frac{1}{2\pi}\int_{-\infty}^{\infty} e^{i\omega x}\gamma^*(\omega)\frac{J_1(i\omega r)}{J_1(i\omega)}\,d\omega,$$

where the integral is taken along the real axis of the transform (ω) plane and

$$2\gamma^*(\omega) = \int_0^{x_{\max}} \bar{F}^2(x)\, e^{-i\omega x}\,dx + \frac{\bar{F}^2_{\max}}{i\omega}\exp(-i\omega x_{\max})$$

from (3.4*b*) and the wall conditions (3.5). The results (3.13), (3.15) and (3.16) then follow [e.g. from the pole contributions of $J_1(i\omega)$].

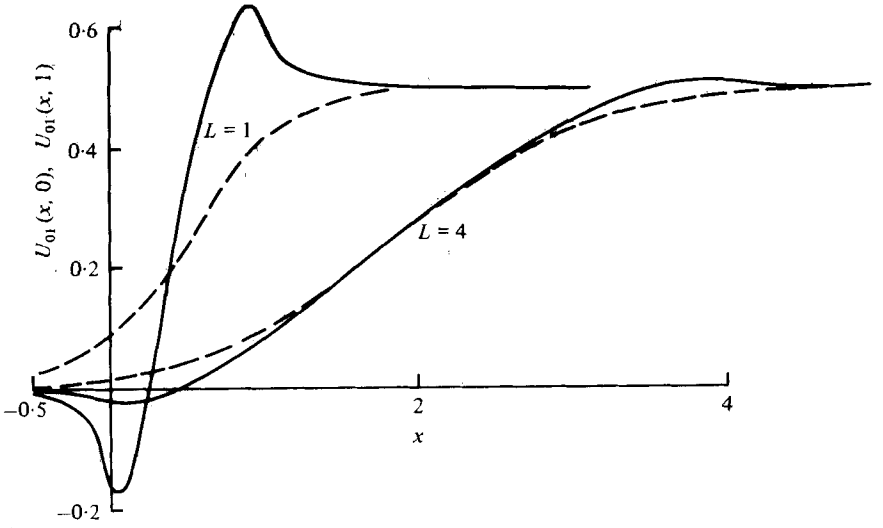

FIGURE 4. The function $u_{01}(x, 1)$ (solid curve) of (3.17*a–c*), giving the (negative of the) free-streamline shape C_0C_1 in $x < 0$ [see (3.4*a*)], and the slip velocity correction in $0 < x < L$ [see (3.3) and (3.4*b*)] for the moderately severe constriction in (3.14), when $L = 1$ or $L = 4$. In $x > L$, $u_{01}(L, 1) - u_{01}(x, 1)$ gives the deviation of the free streamline C_2C_3 from absolute straightness [see (3.4*b*)]. The dashed curve shows the perturbation velocity $u_{01}(x, 0)$ along the centre-line.

Hence, from (3.9) and (3.11),

$$x_1 = \frac{hL}{2^{\frac{1}{2}}} \sum_{n=1}^{\infty} \beta_n \hat{\gamma}_{0n} + O(h^2 \ln h), \quad x_2 = L + \frac{h \ln h}{2^{\frac{1}{2}}\pi} + O(h \ln(-\ln h)). \quad (3.18a, b)$$

The solutions for u_{01} in (3.17) confirm that u_{01} is continuous at $x = 0$ and $x = L$, since

$$\sum_{n=1}^{\infty} \beta_n^{-2} = \frac{1}{8}, \quad \sum_{n=1}^{\infty} \beta_n^{-4} = \frac{1}{192}.$$

They also confirm the singular derivative implied by (3.8) at $x = 0$. The solution curves for the perturbation velocities $u_{01}(x, 1)$ on the surface and $u_{01}(x, 0)$ along the centre-line are given in figure 4. We observe that ψ_{01} and ψ_{02} have singular second derivatives at $x = x_{\max}+$, in agreement with the property that when $x_{\max} - x$ and $1 - r$ are both $O(h)$ the motion is no longer a small perturbation of (1.1), (3.1) then becomes invalid and the pressure gradient retrieves the singular form referred to between (2.9) and (2.10). A similar breakdown of the expansion occurs near the reattachment point x_1. These breakdowns near separation and reattachment affect only the lower-order terms in (3.9)–(3.11). Also, $f_{21}(x)$ in (3.4*b*) is positive (see figure 4), increasing from zero at $x = L$ and tending to 0·105 (for $L = 1$) as $x \to \infty$, so that to $O(h^2)$, $c = 1 - 2^{-\frac{1}{2}}h - 0{\cdot}105h^2$ for $L = 1$. Similarly, $c = 1 - 2^{-\frac{1}{2}}h - 0{\cdot}011h^2$ for $L = 4$.

Solutions of the boundary layer (of thickness $O(R^{-\frac{1}{2}}h^{-\frac{1}{2}})$ when $h \ll 1$) on the constriction shape (3.14) are given by Smith (1977*a*) (the shear stress $\partial u/\partial y$ at the wall reaches a maximum value of $0{\cdot}581h^{\frac{3}{2}}R^{\frac{1}{2}}L^{-\frac{1}{2}}$, at $x = 0{\cdot}605L$) and indeed the first-order flow for h small matches directly with the upper limit of moderately constricted motions. Finally, the constant π_1 required in (2.5)–(2.9) above is given by

$$\pi_1 = \beta_1 \hat{\gamma}_{01} h^2 + O(h^3) \quad (h \ll 1) \quad (3.19)$$

for any shape $\bar{F}(x)$.

4. Very severe constrictions

At the other extreme, for a very severe constriction where the minimum radius $1-F_{\max}$ is small, some analytical details are again forthcoming. We write $1-F_{\max}=\epsilon$, and suppose that, in the gap near the point of minimum radius [i.e. while r is $O(\epsilon)$], the constriction is smooth with its slope dF/dx remaining small. Specifically, suppose that $dF/dx = O(\epsilon^{\frac{1}{2}})$ (this choice gives finite curvature, although the theory below applies for $dF/dx = O(\epsilon^q)$, where $q>0$). Then in the gap the appropriate scalings are $r=\epsilon\hat{r}$, $x=\epsilon^{\frac{1}{2}}\hat{x}+x_{\max}$ and

$$\psi_0 = \hat{\psi}_0(\hat{x},\hat{r})+\epsilon\hat{\psi}_1(\hat{x},\hat{r})+\ldots, \quad u_0=\epsilon^{-2}\hat{u}_0(x,r)+\epsilon^{-1}\hat{u}_1(\hat{x},\hat{r})+\ldots \tag{4.1}$$

since (2.3a, c) require that ψ_0 remains finite for mass conservation. Substituting into (2.2) and (2.3), we have $\partial^2\hat{\psi}_0/\partial\hat{r}^2 = \hat{r}^{-1}\partial\hat{\psi}_0/\partial\hat{r}$, with $\hat{\psi}_0(\hat{x},0)=-\frac{1}{8}$ and $\hat{\psi}_0(\hat{x},\hat{F}_0)=0$. Here

$$F(x) = 1-\epsilon\hat{F}_0(\hat{x}) \tag{4.2}$$

say, and $\hat{F}_0$ is $O(1)$ for $\hat{x}=O(1)$, with $\hat{F}_0(\hat{x})>0$ for all $\hat{x}$ values, to avoid closure of the gap. (If the gap were fully closed the initial condition (1.2) would be inappropriate, of course. Hall & Parker (1976) discuss the sudden closing of a gap.) Hence

$$\hat{\psi}_0 = \tfrac{1}{2}A_0(\hat{x})\hat{r}^2-\tfrac{1}{8}, \quad \hat{u}_0 = A_0(\hat{x}), \tag{4.3}$$

where $A_0(\hat{x}) = 1/4\hat{F}_0^2(\hat{x})$. Therefore the major effect of the very severe constriction is to produce a uniform velocity profile through the gap. Extending the series to lower orders, we find

$$\left.\begin{aligned}\hat{\psi}_1 &= \tfrac{1}{2}A_1(\hat{x})\hat{r}^2-\tfrac{1}{16}A_0''(\hat{x})\hat{r}^4,\\ \hat{\psi}_2 &= \tfrac{1}{2}A_2(\hat{x})r^2-\tfrac{1}{16}A_1''(\hat{x})\hat{r}^4+\tfrac{1}{384}A_0^{\mathrm{iv}}(\hat{x})\hat{r}^6,\end{aligned}\right\} \tag{4.4a}$$

where

$$A_1(\hat{x}) = \tfrac{1}{8}A_0''\hat{F}_0^2, \quad A_2(\hat{x}) = \tfrac{1}{3}\hat{F}_0^2[A_1''-\tfrac{1}{64}A_0^{\mathrm{iv}}\hat{F}_0^2]. \tag{4.4b}$$

Also, from (4.1),

$$U(x) = \frac{\epsilon^{-2}}{4\hat{F}_0^2(\hat{x})}+\epsilon^{-1}\left(A_1-\frac{A_0''\hat{F}_0^2}{4}\right)+\left(A_2-\frac{A_1''\hat{F}_0^2}{4}+\frac{A_0^{\mathrm{iv}}\hat{F}_0^4}{64}\right)+O(\epsilon) \tag{4.5}$$

gives the slip velocity at the constriction surface. Since this cannot yield a deceleration, the separation point occurs when $d\hat{F}_0/d\hat{x}=0$ to leading order, so that $x_2 = x_{\max}+O(\epsilon)$ and, from (4.4) and (4.5),

$$F_2(x) = 1-\epsilon+O(\epsilon^2) \tag{4.6}$$

(since $\hat{F}_0(0)=1$). As in the moderately severe case of § 3, the point of maximum constriction yields separation and beyond there the free streamline C_2C_3 is, to leading order, straight and axial (figure 5). The upstream separation streamline does not lie within the gap zone where $r=O(\epsilon)$, however, from (4.5) (which holds for $-\infty<\hat{x}<0$); so it must be a feature of the grosser-scale upstream motion, as must the match with the initial forms (1.2).

Sufficiently far ahead of the gap the expansion (4.1) becomes invalid in general. If $\hat{F}_0(\hat{x})\propto|\hat{x}|^l$, say (where $l>1$), as $\hat{x}\to-\infty$, then (4.3) and (4.4) suggest breakdown of (4.1) when $|\hat{x}|$ is large and $O(\epsilon^{-1/(2l-2)})$, i.e. when the slope of the constriction becomes finite upstream of the gap. Then r and x both have typical length scales $O(\epsilon^{(l-2)/(2l-2)})$. Therefore the upstream structure is heavily dependent on the particular geometry

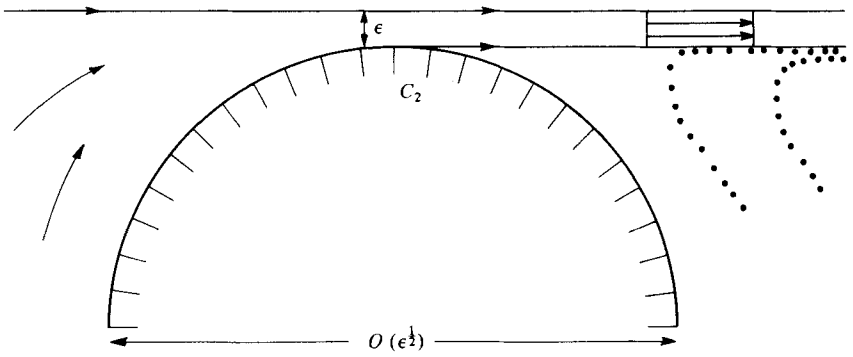

FIGURE 5. The main flow features through the very severe constriction considered in § 4.

of the very severe constriction (see, for example, § 5 below), in contrast with the downstream features. The drag C_D on the constriction is dominated by the low downstream pressure contribution p_{00}, however, and (2.11) yields

$$C_D = \pi/32\epsilon^4 + O(1). \tag{4.7}$$

Also, the boundary layer on the constriction thins to an $O(R^{-\frac{1}{2}}\epsilon^{\frac{5}{2}})$ thickness in the small gap ahead of separation.

Another form of very severe constriction occurs if the body slope is $O(1)$ in the gap. Then $x - x_{\max}$ and r both have typical length scales $O(\epsilon)$. An expansion of the form (4.1) is again appropriate, with $\hat{x}$ replaced by $\bar{x} = \epsilon^{-1}(x - x_{\max})$, but now $\hat{\psi}_0$ satisfies $D^2\hat{\psi}_0 = 0$ [instead of (2.2)] and the Kirchhoff conditions of § 2. Unfortunately, with this sharp-edged constriction solution is by no means straightforward, mainly because the operator D^2 acquires a complicated form (see, for example, Milne-Thompson 1968, chap. XVI) under the conformal mappings which are suitable for the free-streamline conditions, although some qualitative flow properties are given by Batchelor (1967, chap. VI, § 6.3). On the other hand, if we consider the two-dimensional channel flow analogue, then ∇^2 replaced D^2 ($\nabla^2 \equiv \partial^2/\partial\bar{x}^2 + \partial^2/\partial\bar{y}^2$, where $\bar{y}$ denotes non-dimensional distance from the axis of symmetry). Hence the motion through the two-dimensional gap is governed by the classical inviscid theory of jet flow through an aperture (Milne-Thompson 1968, chap. XI), for which solutions are available for simple geometries. For example, if the two-dimensional constriction is a flat plate perpendicular to the x axis, and the minimum gap width is 2ϵ, then it is found that $c = \pi\epsilon/(\pi + 2)$ to leading order in ϵ, where $2c$ is the width of the jet flow far beyond the constriction.

5. Slowly varying severe constrictions

If the typical axial length scale of the entire constriction is large (λ, say), an extension of the simplifying feature in (4.1)–(4.7) can be made to produce a global solution for the motion even for very severe constriction. Suppose that F depends on $X = \lambda^{-1}x$ then, rather than on x, where $\lambda \gg 1$. Then we expand

$$\psi_0 = \psi_0^{(0)}(X, r) + \sum_{n=1}^{\infty} \lambda^{-2n}\psi_0^{(n)}(X, r), \tag{5.1}$$

so that (2.2) reduces to the successive equations

$$(\partial^2/\partial r^2 - r^{-1}\partial/\partial r)\,\psi^{(0)} = -r^2, \tag{5.2a}$$

$$(\partial^2/\partial r^2 - r^{-1}\partial/\partial r)\,\psi_0^{(n)} = -\partial^2\psi_0^{(n-1)}/\partial X^2 \quad (n \geqslant 1). \tag{5.2b}$$

The boundary conditions are

$$\psi_0^{(0)}(X,0) = -\tfrac{1}{8}, \quad \psi_0^{(0)}(X, 1-F(X)) = 0, \tag{5.3a}$$

$$\psi_0^{(n)}(X,0) = 0 = \psi_0^{(n)}(X, 1-F(X)) \quad (n \geqslant 1) \tag{5.3b}$$

on body surfaces, together with the free-streamline conditions (2.3) and (2.4) and $\psi_0^{(0)}(-\infty, r) = \Psi_0(r)$ and $\psi_0^{(n)}(-\infty, r) = 0$ from (2.3d). The solutions for the first two terms are

$$\psi_0^{(0)} = -\tfrac{1}{8}(1+r^4) + \tfrac{1}{8}r^2 f^{-2}(1+f^4), \tag{5.4a}$$

$$\psi_0^{(1)} = \tfrac{1}{16}r^2 A_0''(X)\,(f^2 - r^2), \tag{5.4b}$$

where $A_0(X) = \frac{1}{4}(f^2 + f^{-2})$ and $f = 1 - F(X)$ at axial stations where the flow is attached. But (5.4a, b) give the slip velocity

$$U(x) = \tfrac{1}{4}(f^{-2} - f^2) - \tfrac{1}{8}A_0''(X) f^2 \lambda^{-2} + O(\lambda^{-4}), \tag{5.5}$$

which would yield deceleration in $x > x_{\max}$. Therefore separation is implied when $x = x_2 = x_{\max} + O(\lambda^{-2})$, again at the maximum constriction point (cf. (3.11a) and § 4). Beyond $x = x_{\max}$ we require $U(x)$ to be uniform, so that from (5.5)

$$F_2 = F_{\max} + O(\lambda^{-2}) \tag{5.6}$$

and the free streamline C_2C_3 is again straight (to leading order in λ^{-1}). Clearly these results, summarized in figure 6, can be extended to higher order in λ^{-1} and they include as a special case the local properties of very severely constricted flows in § 4. However, to determine the reattachment position x_1 and upstream separation constant π_1 in (2.9), a shorter-scale study (given below) is required, since, on the long scale $O(\lambda)$, the upstream free streamline C_0C_1 does not appear. It is confined to the vicinity of the onset of constriction ($X = 0+$), where a slight discontinuity is present since, according to (5.4), the flow is completely unaltered from the incoming form (1.2) ahead of the constriction ($X < 0$). There, if $F \sim K_0 X + O(X^2)$, where K_0 (> 0) is a constant, then the series (5.5), for instance, eventually breaks down. The smoothing out of the discontinuity at $X = 0$ takes place on the finite length scale of x and r. On this scale the constriction has the shape $F = \lambda^{-1}K_0 x + O(\lambda^{-2})$ for $x > 0$, so the moderately severe analysis of § 3 applies with $h = \lambda^{-1}K_0$ ($\ll 1$) and $\bar{F}(x) = x$ for $x > 0$. From (3.13)–(3.17) we have

$$\psi_{01} = \begin{cases} -r \sum_{n=1}^{\infty} \dfrac{\exp(\beta_n x) J_1(\beta_n r)}{\beta_n^3 J_1'(\beta_n)} & \text{for} \quad x < 0, \qquad (5.7a) \\ r^2\left[\dfrac{x^2}{2} + \dfrac{1-r^2}{8}\right] + r \sum_{n=1}^{\infty} \dfrac{\exp(-\beta_n x) J_1(\beta_n r)}{\beta_n^3 J_1'(\beta_n)} & \text{for} \quad x > 0, \qquad (5.7b) \end{cases}$$

$$u_{01} = -\sum_{n=1}^{\infty} \frac{\exp(\beta_n x)}{\beta_n^2} \quad (x < 0) \quad \text{or} \quad x^2 - \tfrac{1}{4} + \sum_{n=1}^{\infty} \frac{\exp(-\beta_n x)}{\beta_n^2} \quad (x > 0) \tag{5.8}$$

and from (3.9)

$$x_1 = \frac{1}{8}\left[\frac{K_0}{\lambda} - \frac{K_0^2}{\pi\lambda^2}\ln\left(\frac{K_0}{\lambda}\right)\right] + O(\lambda^{-2}). \tag{5.9}$$

Also,

$$\pi_1 = K_0^2/\beta_1^2\lambda^2 + O(\lambda^{-3}) \tag{5.10}$$

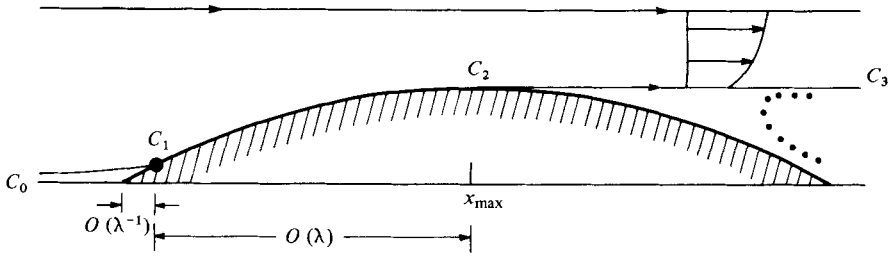

FIGURE 6. Flow structure produced by a slowly varying severe constriction.

fixes the upstream separation position of (2.9). As $x \to \infty$ the merging with (5.4) and (5.5) is achieved by (5.7) and (5.8). The reattachment point C_1 is at a distance $O(\lambda^{-1})$ from the onset of constriction, whereas the separation point C_2 is a feature of the broader-scale flow (5.1)–(5.6). The drag C_D also depends on (5.1)–(5.6) but to leading order is given by (2.11) with c replaced by $1 - F_{\max}$ [from (5.6)]. Like § 3 the above provides a complete description of the motion, apart from the vicinities of the reattachment and separation points C_1 and C_2.

6. Suppression of upstream separation

The main cause of the upstream separation [in (1.1) or (2.9)] in the above severely constricted tubes is the fact that the constrictions have a definite starting point, so that far upstream the flow response is of the eigenfunction form (2.5), for which separation is inevitable. Similarly the form (2.5) would dominate (and produce separation) if the constriction $F(x)$ did not have a definite starting point but nevertheless decayed upstream faster than $\exp(\beta_1 x)$. On the other hand, if the constriction decays slower than $\exp(\beta_1 x)$ then the far upstream disturbances are of the forced type, for which separation is suppressed, as follows.

Let us examine, then, an algebraic decay far upstream of the type

$$F(x) \sim \mu |x|^{-N} \quad \text{for} \quad x \to -\infty, \tag{6.1}$$

where the constant $\mu > 0$ for constriction, and $N > 0$. Then the solution of (2.2) as $x \to -\infty$ gives

$$\psi_0 = \Psi_0(r) - \tfrac{1}{2}\mu^2 r^2 |x|^{-2N} + o(|x|^{-2N}), \tag{6.2a}$$

$$U(x) = \mu |x|^{-N} + o(|x|^{-N}), \tag{6.2b}$$

so the slip velocity is accelerating and attached flow is implied upstream. However, a nonlinear viscous adjustment is still necessary ahead of the $x = O(1)$ regime because ultimately (6.2*b*) and the oncoming velocity in (1.2) must become comparable near the wall. Below we consider first (in §§ 6.1 and 6.2) this nonlinear adjustment. Its properties then lead us on to consider (§ 6.3) a further necessary (but linear) adjustment which occurs on an even longer scale upstream. The complete flow structure is shown in figure 7.

6.1. *The nonlinear viscous adjustment upsteam*

This upstream adjustment takes place on a large axial length scale, unlike that in § 2, where the exponential decay demands an $O(1)$ scaling. The required balancing of

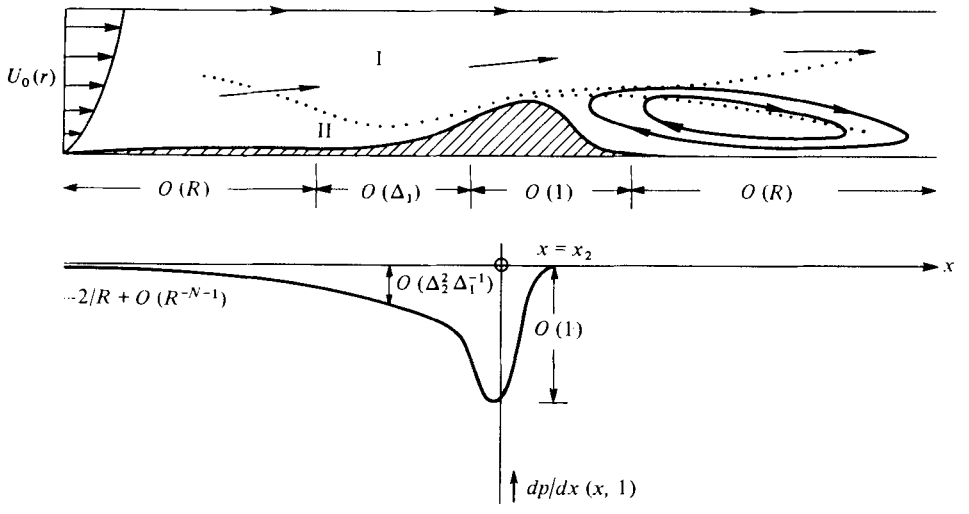

FIGURE 7. Sketch (not to scale) of the different flow regions studied in § 6, where upstream separation is suppressed. The dots indicate the edges of the viscous layer II, whose thickness is $O(\Delta_2)$, $O(R^{-\frac{1}{2}})$ and $O(1)$ for $-x = O(\Delta_1)$, $x = O(1)$ and $x = O(R)$ respectively. Shown underneath is the variation of the wall pressure gradient through the tube (for $0 < N < \frac{1}{3}$).

inertial and viscous forces in a wall layer, with the oncoming motion (1.2) disturbed nonlinearly, demands an axial length scale $O(\Delta_1 = R^{1/(1+3N)})$ and a wall-layer thickness $O(\Delta_2 = R^{-N/(1+3N)})$.

Setting $x = \Delta_1 X$, where X is finite but negative, we have

$$u = \Delta_2 U_{\rm II}, \quad \psi = -\Delta_2^2 \Psi_{\rm II}, \quad p = \Delta_2^2 P_{\rm II} \tag{6.3}$$

in the wall layer II, where $r = 1 - \Delta_2 Z_{\rm II}$ and $Z_{\rm II}$ is $O(1)$. The flow in layer II is controlled by the boundary-layer equations (where we introduce for convenience the Prandtl transformation $\bar{Z} = Z_{\rm II} - \mu|X|^{-N}$)

$$U_{\rm II} = \frac{\partial \Psi_{\rm II}}{\partial \bar{Z}}, \quad U_{\rm II}\frac{\partial U_{\rm II}}{\partial X} - \frac{\partial \Psi_{\rm II}}{\partial X}\frac{\partial U_{\rm II}}{\partial \bar{Z}} = -\frac{dP_{\rm II}}{dX} + \frac{\partial^2 U_{\rm II}}{\partial \bar{Z}^2}, \quad P_{\rm II} = P_{\rm II}(X), \tag{6.4a}$$

with the boundary conditions

$$U_{\rm II} = \Psi_{\rm II} = 0 \quad \text{at} \quad \bar{Z} = 0, \tag{6.4b}$$

$$U_{\rm II} \to \bar{Z}, \quad \Psi_{\rm II} \to \tfrac{1}{2}\bar{Z}^2, \quad dP_{\rm II}/dX \to 0 \quad \text{as} \quad X \to -\infty \quad \text{with } \bar{Z} \text{ fixed}, \tag{6.4c}$$

$$\left.\begin{aligned} \Psi_{\rm II} &\sim \tfrac{1}{2}(\bar{Z} + \mu|X|^{-N})^2 + P_{\rm II}(X) + \ldots \\ U_{\rm II} &\sim \bar{Z} + \mu|X|^{-N} + \ldots \end{aligned}\right\} \quad \text{as} \quad \bar{Z} \to \infty \quad \text{with } X \text{ fixed}. \tag{6.4d}$$

Here (6.4*b*) is the no-slip condition on the disturbed wall and (6.4*c*) represents the initial profile (1.2). Finally, (6.4*d*) joins the wall-layer flow to the core flow I, wherein r is $O(1)$ and (provided $N > \frac{1}{3}$; see (6.15) below)

$$\psi = \Psi_0(r) - \Delta_2^2 P_{\rm II}(X) r^2 + o(\Delta_2^2) \tag{6.5}$$

from the Navier–Stokes equations and the symmetry condition $\psi(X, 0) = -\frac{1}{8}$. The merging into the asymptotic form (6.4*d*) is algebraic (as with Brown & Stewartson

1970; Melnik & Chow 1975; Smith 1977*b*) rather than exponential. Likewise, the starting form in II, for X large and negative, has the algebraic similarity properties

$$\Psi_{\rm II} \sim \tfrac{1}{2}|X|^{\frac{2}{3}}\eta^2 + |X|^{\frac{1}{3}-N}\mathscr{F}_0(\eta), \quad U_{\rm II} \sim |X|^{\frac{1}{3}}\eta + |X|^{-N}\mathscr{F}_0'(\eta), \quad P_{\rm II} \sim P_0|X|^{\frac{1}{3}-N}, \tag{6.6}$$

where $\eta = \bar{Z}|X|^{-\frac{1}{3}}$ is $O(1)$ and $\mathscr{F}_0(\eta)$ satisfies

$$\mathscr{F}_0''' - \tfrac{1}{3}\eta^2\mathscr{F}_0'' + (\tfrac{1}{3}-N)(\eta\mathscr{F}_0' - \mathscr{F}_0 + P_0) = 0, \tag{6.7a}$$

$$\mathscr{F}_0(0) = \mathscr{F}_0'(0) = 0, \quad \mathscr{F}_0'(\infty) = \mu. \tag{6.7b}$$

The major features of the solution for $\mathscr{F}_0(\eta)$ depend on the value of N, since (6.7*a*, *b*) yield, on integration,

$$\mathscr{F}_0(\eta) = P_0\left[1 + \frac{9^{N-\frac{1}{3}}\eta}{\Gamma(\frac{2}{3})}\int_0^\eta dq_2 \int_0^\infty q_1^{N-\frac{2}{3}}(1+9q_1)^{\frac{1}{3}-N}\exp\left[-q_1 q_2^3\right]dq_1\right], \tag{6.8a}$$

where the integral is to take its finite part and

$$P_0 = -3^{\frac{5}{3}}\mu\Gamma(N+\tfrac{2}{3})/\Gamma(\tfrac{1}{3})\,\Gamma(N)\,(3N-1). \tag{6.8b}$$

Hence, if $N > \frac{1}{3}$, $P_0 < 0$ with $|P_{\rm II}(X)| \to 0$ as $X \to -\infty$, while if $N < \frac{1}{3}$, $P_0 > 0$ with $|P_{\rm II}(X)| \to \infty$ as $X \to -\infty$. In either case the pressure gradient is favourable (the trivial case $N = \frac{1}{3}$ gives also an increasing, logarithmic, pressure as X decreases), and the series (6.6), with (6.8*a*, *b*), yield the increasing skin friction

$$\tau_{\rm II}(X) \equiv \frac{\partial U_{\rm II}}{\partial \bar{Z}}(X,0) \sim 1 + \frac{3^{\frac{1}{3}}\Gamma(N+\frac{1}{3})\,\mu}{\Gamma(N)\,\Gamma(\frac{2}{3})}|X|^{-N-\frac{1}{3}} \tag{6.8c}$$

in accord with the pressure gradient. But an important distinction does arise between the two cases $N \lessgtr \frac{1}{3}$, since for $\eta \gg 1$

$$\mathscr{F}_0(\eta) \sim \mu\eta + P_0 + \mu\eta^{1-3N}\frac{\Gamma(N+\frac{1}{3})\,\Gamma(N+\frac{2}{3})\,3^{2N+\frac{1}{2}}}{2\pi N(3N-1)\,\Gamma(N)} + \ldots. \tag{6.9}$$

So if $N > \frac{1}{3}$ the pressure term P_0 dominates the perturbations to the uniform stream $F_0 = \mu\eta$ and the third term in (6.9) implies only a minor contribution $O(Z^{1-3N})$ to the outer condition on $\Psi_{\rm II}$ in (6.4*d*). The core flow in (6.5) is then consistent with (6.4*d*). The work in § 6.2 will be concerned with the case $N > \frac{1}{3}$; the case $0 < N \leqslant \frac{1}{3}$ requires extra attention and leads to the further upstream adjustment considered in § 6.3 below.

6.2. *The solution in II*

The necessarily numerical solution of (6.4*a–d*), which fixes the upstream adjustment in I and II, was determined for a number of values of N using a centred-difference scheme similar to those of Smith (1977*a–c*). In practice, to incorporate the singular starting form (6.6)–(6.9) into the calculations it proved best to integrate (6.7) numerically for $\mathscr{F}_0(\eta)$, along with one extra term in the series of (6.6). When the calculated flow in II carries on from (6.6) for finite values of X the skin friction $\tau_{\rm II}(x)$ and pressure $P_{\rm II}(X)$ continue their respective upward and downward trends (figure 8). Mesh widths $\Delta X = 0{\cdot}02$ and $\Delta\bar{Z} = 0{\cdot}1$, a starting position $X = X_{-\infty} = -20$ and a Newton iterative tolerance of 10^{-7} were sufficient in general for an accuracy of four significant figures in $P_{\rm II}(X)$.

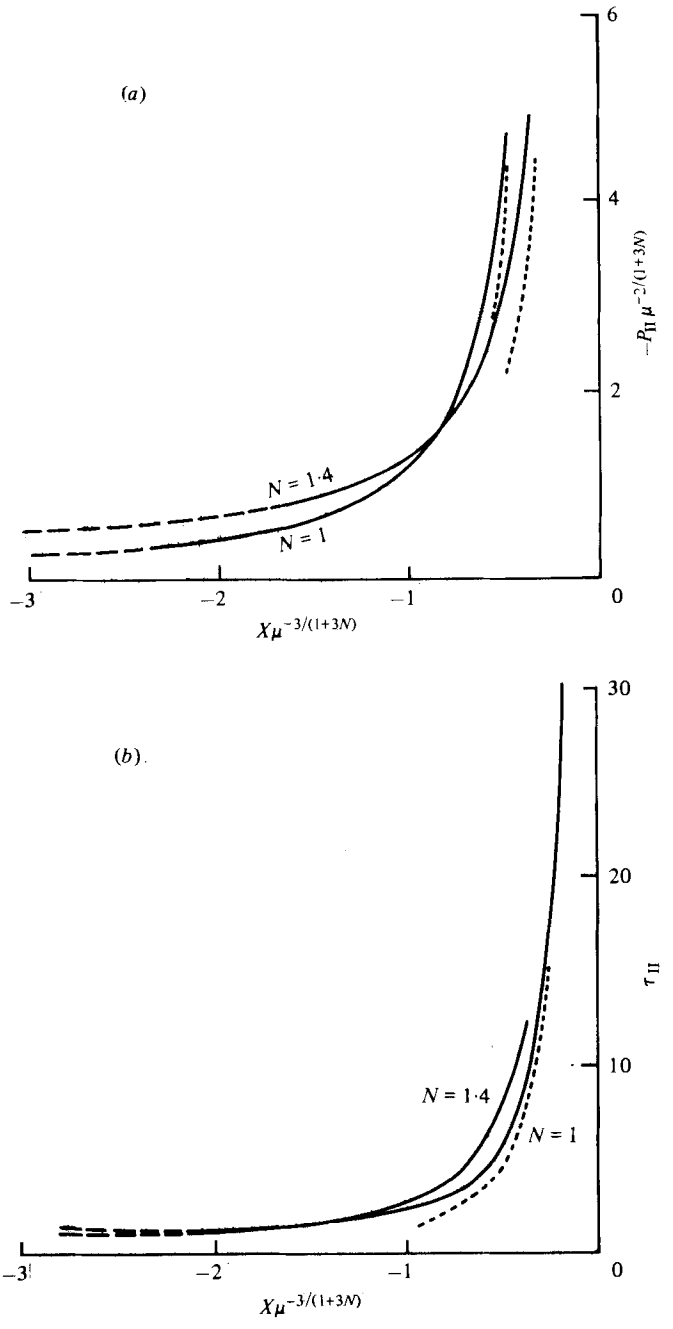

FIGURE 8. (*a*) Pressure $P_{II}(X)$ and (*b*) skin friction $\tau_{II}(X)$ for the upstream response studied in (6.3)–(6.16), with $N = 1, 1{\cdot}4$. Asymptotes: – – –, from (6.6); · · · ·, from (6.12)–(6.16).

As X approaches zero the singularities in (6.4d) assert themselves (since on this scale the majority of the constriction acts as a singularity at $X = 0-$). The structure of II near $X = 0-$ is similar to that of Stewartson (1970b) except that here the effective displacement ($\mu|X|^{-N}$) is prescribed. An analysis along his lines is relevant. For $X \to 0-$ the solution given by the constraint (6.4d) holds for all finite positive values of $\bar{Z}$, so that

$$\Psi_{\rm II} \sim \tfrac{1}{2}(Z+\mu|X|^{-N})^2 + P_{\rm II}(X), \quad U_{\rm II} \sim \bar{Z} + \mu|X|^{-N} \quad \text{for} \quad \bar{Z} > 0. \tag{6.10}$$

The condition (6.4b) is violated by (6.10), of course, and a slip layer is required near $\bar{Z} = 0$, wherein $\xi = \bar{Z}\mu^{\frac{1}{2}}/|X|^{\frac{1}{2}(1+N)}$ is $O(1)$. Here

$$\Psi_{\rm II} \sim |X|^{\frac{1}{2}(1-N)} F_{\rm II}(\xi)\mu^{\frac{1}{2}} + \ldots, \quad U_{\rm II} \sim |X|^{-N} F'_{\rm II}(\xi)\mu + \ldots, \tag{6.11}$$

implying

$$P_{\rm II}(X) \sim -\tfrac{1}{2}\mu^2|X|^{-2N} \tag{6.12}$$

for consistency, and $F_{\rm II}(\xi)$ satisfies the Falkner–Skan problem

$$F'''_{\rm II} + \tfrac{1}{2}(N-1)F_{\rm II}F''_{\rm II} + N(1-F'^2_{\rm II}) = 0, \tag{6.13a}$$

$$F_{\rm II}(0) = F'_{\rm II}(0) = 0, \quad F'_{\rm II}(\infty) = 1 \tag{6.13b, c}$$

The outer condition (6.13c) matches (6.11) (as $\xi \to \infty$) with (6.10) (as $\bar{Z} \to 0+$). The solution of (6.13), like that of (6.7), depends on the value of N but it exists for all positive N. (See Jones & Watson 1963, p. 250; their α and β take the values sgn $(N-1)$ and $2N/|N-1|$ respectively if $N \neq 1$ and the values zero and 1 if $N = 1$. In all cases the velocity profile $F'_{\rm II}$ increases monotonically from zero to unity as ξ increases.) The main property from (6.13) is the form of the skin friction

$$\tau_{\rm II}(X) \sim |X|^{-\frac{1}{2}(3N+1)} F''_{\rm II}(0)\mu^{\frac{3}{2}} \quad \text{for} \quad X \to 0-. \tag{6.14}$$

Further terms in (6.10)–(6.12) are readily obtained. However, comparisons given in figure 8 of (6.10)–(6.14) with the numerical solutions tend to confirm the singular behaviour.

Reconsidering the necessary match with the flow (6.2a, b) when x is $O(1)$, we see that (6.10)–(6.14) are consistent. For example, the core of (6.5) merges with (6.2a), via (6.12). Again, the viscous part of the wall layer II has thickness $\Delta_2|X|^{\frac{1}{2}(1+N)}$ as $X \to 0-$, which converts to $R^{-\frac{1}{2}}|x|^{\frac{1}{2}(1+N)}$ for $x \to -\infty$, and the classical $R^{-\frac{1}{2}}$ order is as expected for the severe constriction (see, for example, § 2) when x becomes finite.

Similar long-scale upstream adjustments occur for exponentially decaying constrictions, rather than (6.1), and for decaying dilatations where μ would be negative in (6.1). In the latter, however, the structure is similar to that in Smith (1977c) and separation occurs for a finite negative value of X. Hence a slow upstream decay in a dilatation fails to suppress separation (and the original flow (1.2) tends to continue forward in the axial direction, leaving a slow eddying motion to fill the dilatation), in contrast with the suppression of separation by slow upstream decay in a constriction.

6.3. *The linear adjustment at distances $O(R)$ upstream*

The above solution features in I and II as $X \to 0-$ hold for all $N > 0$, but we need to reconsider, finally, the odd properties of the cases $0 < N \leqslant \frac{1}{3}$ when $X \to -\infty$. For, if $N < \frac{1}{3}$, the term $O(\eta^{1-3N})$ in (6.9) dominates the pressure term and forces a

contribution $O(Z^{1-3N})$ in $\Psi_{\rm II}$ in (6.4d) for all X (<0). Since this dominates the pressure in (6.4d), the core of (6.5) is incomplete and a supplemented expansion

$$\left.\begin{aligned}\psi &= \Psi_0(r)+R^{-N}\hat{\psi}_1(X,r)-\Delta_2^2 r^2 P_{\rm II}(X)+o(\Delta_2^2),\\ u &= U_0(r)+R^{-N}\hat{u}_1(X,r)-2\Delta_2^2 P_{\rm II}(X)+o(\Delta_2^2)\end{aligned}\right\} \tag{6.15}$$

should replace (6.5). But substitution into the Navier–Stokes equations and the axisymmetry condition yield $\partial\hat{\psi}_1/\partial X = 0$, giving

$$\hat{\psi}_1 = \hat{\psi}_1(r), \quad \hat{u}_1 = \hat{u}_1(r) \quad \text{for all} \quad X < 0. \tag{6.16a}$$

The profile $\hat{u}_1(r)$ cannot be determined from the present (I–II) structure, but is certainly non-zero since we require

$$\hat{u}_1(r) \sim -\mu\frac{\Gamma(N+\frac{1}{3})\,\Gamma(N+\frac{2}{3})\,3^{2N+\frac{1}{2}}}{2\pi N\Gamma(N)}(1-r)^{-3N} \quad \text{as} \quad r\to 1- \tag{6.16b}$$

to match with (6.9). However, there is now a mismatch with the upstream conditions (1.2); so how does the arbitrary profile (6.16a) evolve? The question of the arbitrary profile also arises if $N = \frac{1}{3}$, when the $O(\eta^{1-3N})$ term in (6.9) is replaced by a $\ln\eta$ term. Therefore all the constrictions with $0 < N \leqslant \frac{1}{3}$ require further attention as far as their properties for $X\to-\infty$ are concerned. (A less pronounced mismatch occurs if $N > \frac{1}{3}$.) We find that in fact the profile (6.16a) is generated from (1.2) through an extra upstream adjustment on an even longer axial scale than $O(\Delta_1)$, namely $O(R)$. On that scale viscous effects fill the entire tube because, for example, the thickness of II, $\Delta_2|x\Delta_1^{-1}|^{\frac{1}{3}}$ for $X\to-\infty$ from (6.6), increases to $O(1)$ when x is $O(R)$ and negative. Let us take the example $N = \frac{1}{6}$, for clarity. Then, when $x = Rx^*$ with $x^* = O(1)$ but negative, the solution has the uniform expansion

$$\left.\begin{aligned}\psi &= \Psi_0(r)+R^{-\frac{1}{6}}\psi^*(x^*,r)+O(R^{-\frac{1}{3}}),\\ u &= U_0(r)+R^{-\frac{1}{6}}u^*(x^*,r)+O(R^{-\frac{1}{3}}),\\ p &= -2x^*+R^{-\frac{1}{6}}p^*(x^*,r)+O(R^{-\frac{1}{3}})\end{aligned}\right\} \tag{6.17}$$

implied by both (6.16a) and the $O(R^{-\frac{1}{3}})$ wall disturbance from (6.1). The Navier–Stokes equations yield the viscous governing equations

$$u^* = \frac{1}{r}\frac{\partial\psi^*}{\partial r}, \quad U_0(r)\frac{\partial u^*}{\partial x^*}-\frac{U_0'(r)}{r}\frac{\partial\psi^*}{\partial x^*} = -\frac{dp^*}{dx^*}+\frac{\partial^2 u^*}{\partial r^2}+\frac{1}{r}\frac{\partial u^*}{\partial r}, \quad p^* = p^*(x^*) \tag{6.18a}$$

for the disturbances, in $x^* < 0$ and $0 \leqslant r \leqslant 1$. The boundary conditions are

$$\psi^*(x^*,0) = 0, \tag{6.18b}$$

$$\psi^*(x^*,1) = 0, \quad u^*(x^*,1) = -\mu|x^*|^{-\frac{1}{6}} \tag{6.18c}$$

from axisymmetry and the no-slip conditions at the surface (1.3). The starting conditions (1.2) imply that

$$\psi^*(-\infty,r) = 0 = u^*(-\infty,r) = p^{*\prime}(-\infty) \tag{6.18d}$$

and (6.18a–d) fix the solution for ψ^*, u^* and p^* in $x^* < 0$. As $x^*\to 0-$ the only consistent behaviour for (6.18a–c) is the singular form

$$\left.\begin{aligned}\psi^* &\sim \hat{\psi}_1(r)+|x^*|^{\frac{1}{6}}\hat{\psi}_2(r)+O(|x^*|^{\frac{1}{3}}),\\ u^* &\sim \hat{u}_1(r)+|x^*|^{\frac{1}{6}}\hat{u}_2(r)+O(|x^*|^{\frac{1}{3}}),\\ p^{*\prime} &\sim -\tfrac{1}{6}P_0|x^*|^{-\frac{5}{6}}+O(|x^*|^{-\frac{2}{3}}),\end{aligned}\right\} \tag{6.19a}$$

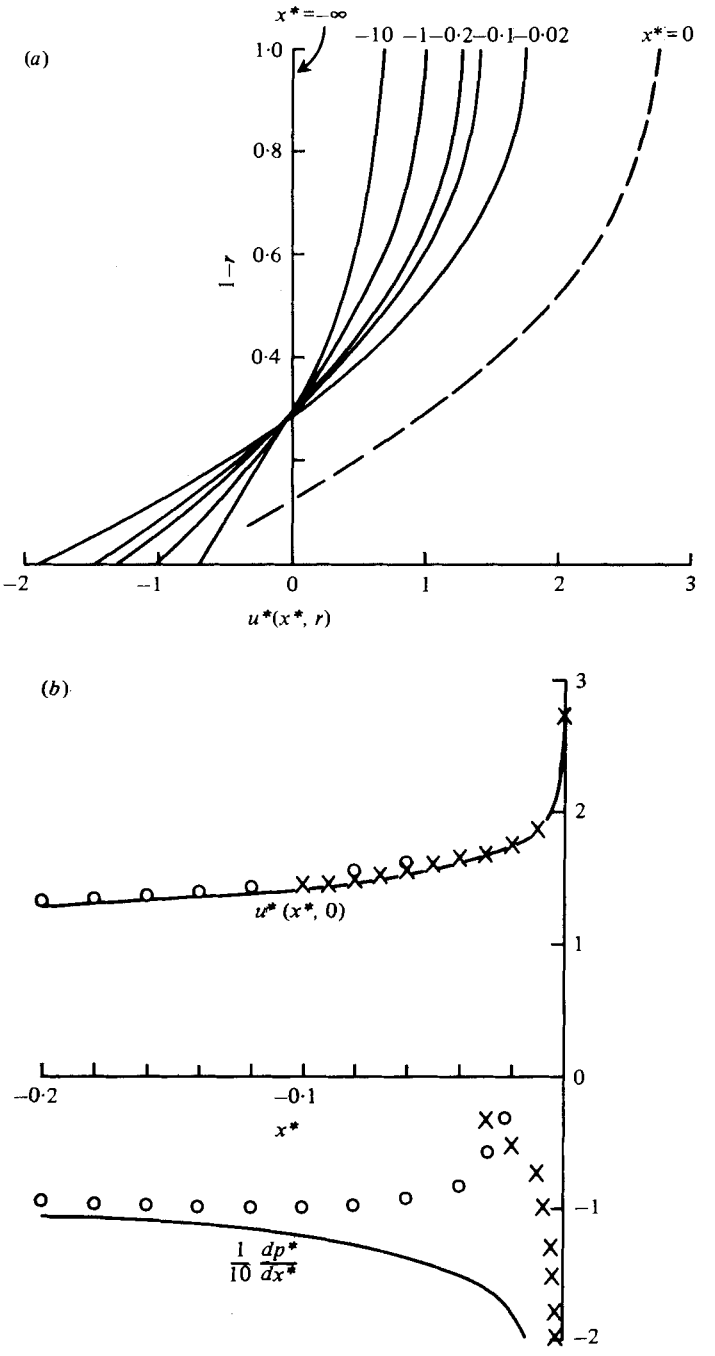

FIGURE 9. (*a*) Calculated velocity profiles (solid curves) for (6.18*a*–*d*) and the terminal form $u_1(r)$ (dashed curve) extrapolated from (6.19*a*, *b*). (*b*) Solution for the long-scale pressure gradient $p^{*\prime}(x^*)$ and centre-line velocity $u^*(x^*, 0)$ in (6.18)–(6.22) ($N = \frac{1}{6}$). Asymptotes: ○, from (6.20); ×, from (6.19*a*).

where, from (6.18*a–c*), the profiles $\hat{u}_1(r)$ and $\hat{\psi}_1(r)$ are undetermined locally [they depend on the whole upstream motion of (6.18*a–d*)] but

$$\hat{\psi}_2 = -P_0 r^2, \quad \hat{u}_2 = -2P_0. \tag{6.19b}$$

A viscous sublayer of thickness $O(|x^*|^{\frac{1}{3}})$ also develops near the wall, to correct for the slip induced by (6.19*a*, *b*). Its characteristics are essentially those of (6.6).

Hence as $x^* \to 0-$ the match with (6.15) and (6.16) (as $X \to -\infty$) is achieved. To verify that the $O(R)$ scaled adjustment can also achieve the necessary joining to the original Poiseuille flow upstream we must consider how the condition (6.18*d*) is effected. We find that, for $x^* \to -\infty$,

$$\psi^* \sim \sum_{n=0}^{\infty} |x^*|^{-n-\frac{1}{6}} f_n^*(r), \quad u^* \sim \sum_{n=0}^{\infty} |x^*|^{-n-\frac{1}{6}} g_n^*(r), \quad p^{*\prime} \sim -\sum_{n=0}^{\infty} (\tfrac{5}{6}-n) p_n^* |x^*|^{-n-\frac{1}{6}}, \tag{6.20}$$

where, from (6.18*a–c*), $rg_n^*(r) = f_n^{*\prime}(r)$ $(n \geqslant 0)$ and

$$\left.\begin{aligned} g_0^{*\prime\prime} + r^{-1} g_0^{*\prime} &= -\tfrac{1}{6} p_0^*, \\ g_n^{*\prime\prime} + r^{-1} g_n^{*\prime} &= (n-\tfrac{5}{6})[p_n^* + U_0 g_{n-1}^* - U_0' r^{-1} f_{n-1}^*] \quad (n \geqslant 1) \\ g_0^*(1) = -\mu, \quad g_n^*(1) &= 0 \quad (n \geqslant 1), \\ f_n^*(0) = f_n^*(1) &= 0 \quad (n \geqslant 0). \end{aligned}\right\} \tag{6.21}$$

An integral formula for f_n^* and g_n^* can be written down. We find in particular that

$$\left.\begin{aligned} p_0^* &= \tfrac{48}{5}\mu, \quad g_0^* = -\mu - \frac{5p_0^*}{24}(r^2-1), \\ p_1^* &= \tfrac{3}{4}\mu, \quad g_1^* = \frac{\mu}{288}\left[24\left(-\frac{r^2}{2}+\frac{r^4}{5}\right) - 6r^2 - 2r^6 + 3r^4 + 11\right] - \frac{p_1^*}{24}(1-r^2), \end{aligned}\right\} \tag{6.22}$$

so that (6.18*d*) is satisfied.

Therefore both extreme conditions (1.2) and (6.15) are met on the $O(R)$ scale. The solution of (6.18*a–d*) describes a buffer zone between (1.2) and the I–II structure of (6.3)–(6.5) in much the same way that the I–II structure provides a buffer between (6.3)–(6.5) and the flow at finite distances from the majority of the constriction. The solutions (determined numerically) for the pressure gradient dp^*/dx^*, centre-line velocity $u^*(x^*, 0)$ and velocity profiles $u^*(x^*, r^*)$ are drawn in figure 9, along with the asymptotes from (6.19*a*) and (6.20)–(6.22). More generally, figure 7 follows the pressure variation through the tube when a constriction having the property (6.1), with $0 < N < \frac{1}{3}$, is present. The pressure gradient changes drastically through the various flow regions. When $N = \frac{1}{6}$, for example, it is equal to $-2R^{-1} + O(R^{-\frac{7}{6}})$ while $x\,(<0)$ is $O(R)$, $O(R^{-\frac{8}{9}})$ when $x\,(<0)$ is $O(R^{\frac{2}{3}})$, $O(1)$ for $x = O(1)$ with $x < x_2$, and $O(R^{-1})$ for $x = O(1)$ when $x > x_2$. Finally, it is $O(R^{-1})$ again during the final reattachment process where x is $O(R)$ and positive.

7. Further discussion

The high Reynolds number flow solutions for moderately severe, very severe or slowly varying severe constrictions seem to provide insight, over a fairly wide range of conditions, into the basic features of the free-streamline problem posed in § 2. One

marked property of all those cases is the appearance of viscous separation (and inviscid breakaway) close to the point of maximum constriction. This property is in line with some experimental observations (Föttinger 1939; Lee & Fung 1970, 1971; Deshpande *et al.* 1976; see also the appendix). Like many other aspects of the motions, it follows from the remarkably simple relations between the obstacle shape and the pressure or slip velocity induced, as in (3.6) and (3.8), (4.5) and (5.5). These relations, in turn, are a direct consequence of the assumption that the incoming profile is of a realistic kind [e.g. (1.3)], with no slip at the tube wall. An unrealistic (e.g. uniform) profile could well lead to unnecessarily complicated relations and/or to misleading predictions for separation and reattachment, we believe. Again, the occurrence of separation near maximum constriction contrasts with the situation in external flows, where separation usually occurs well onto the forward face of a body (Brodetsky 1923; Woods 1955). This delay of separation, like the occurrence of separation far upstream [in (2.9)], is due to the confinement of the flow.

Apart from the predicted positions (C_0, C_1, C_2 in figure 1) of separation and reattachment, and the width c of the jet downstream, perhaps the most representative feature of the flow is the drag C_D (see (2.11) and figure 3). In all the cases studied in §§ 3–5, C_D is given by (2.11) but, since the jet width is equal asymptotically to the minimum tube width, c may be replaced by $1-F_{\max}$ to leading order. On the other hand, there is the possibility of a non-uniqueness arising if the obstacle is very smooth beyond the maximum constriction point, since a conventional boundary layer on the obstacle may be able to stay attached there. This would lead to a much reduced drag. The same possibility occurs in external flows (see, for example, Roshko 1967), although the alternative, attached flow can be discounted if, as in our problems, the obstacle terminates suddenly. Separation can also be suppressed ahead of a severe constriction (§ 6), but only if the constriction has no definite starting point and decays slowly enough upstream.

Comparisons of the theory with solutions of the Navier–Stokes equations and with experiment are presented in the appendix, and they tend to support the high Reynolds number structure proposed.

The relevance of this tube flow study, and of the moderate- and fine-constriction theories (Smith 1976*a*, *b*, 1977*a*), to physiology and engineering is clear. It may be that, with alternative profiles to (1.2), some connexion could also be established with the effects of wall interference in wind-tunnel boundary-layer experiments. The work by Bates (1978) and Smith (1976*d*) may also be applicable to wind-tunnel interference in quasi-unbounded conditions. For all these applications it is noted that the two-dimensional symmetric problem (cf. Tillett 1968) is the same in essence as the axisymmetric problem studied above. However, asymmetric two- or three-dimensional tube flows with severe constrictions have different characteristics. The considerable upstream response in the former case has been examined by Smith (1977*c*) and can no doubt be extended to provide the entire free-streamline description through the constriction; but the account of asymmetric three-dimensional tube flows, probably the most practically important case, has not been advanced beyond the stage of a fine constriction yet. A nonlinear upstream response is generated there (Smith 1976*c*) but its ultimate form, to be determined numerically, is still unknown. On the other hand, it may be foreseen that, for a severely constricted asymmetric tube, free-streamline theory will again provide the basis for the flow description. Another

situation still to be investigated is that of the axisymmetric severe constriction when the axial and radial length scales are comparable but small, and the incoming motion is virtually a uniform shear locally.

I am very grateful to the referees for their interest and constructive comments, for pointing out errors in the original versions of (2.11) and (3.10), and for noting the paper of Deshpande *et al.* (1976).

Appendix. Comparisons with experiments and with Navier–Stokes solutions

Quantitative comparisons of the present theory with experiments (Young & Tsai 1973) and with calculations of the Navier–Stokes equations (Deshpande *et al.* 1976) are given in figures 10(*a*)–(*c*). With one exception (figure 10*c*) our limit solutions for $R \to \infty$ are taken from the slowly varying theory of § 5, since all the constriction shapes $M0$, $M1$, $M2$ and $M3$ considered by Deshpande *et al.* (1976) seem to be of the slowly varying severe kind rather than moderately severe.

Figure 10(*a*) presents the pressure drop PDR ($= 16\Delta p$, where Δp is the difference in pressure p at stations ± 8 pipe diameters from the maximum constriction) as a function of the Reynolds number. Here PDR and $Re = \frac{1}{2}R$ are the variables of figure 6 of Deshpande *et al.* The trends of both the Navier–Stokes solutions and the experiments as Re increases are very close to our limiting solutions (for $16\Delta p_0$ for $Re \gg 1$) for PDR, certainly for the shapes $M0$, $M2$ and $M3$. For the shape $M1$ the experiments suggest a Reynolds number effect persisting above $Re = 1000$, possibly because the major separation (at $x = x_2$) does not appear until $Re = 195$ and $M1$ is the most slowly varying of these constrictions. In figure 10(*b*) the centre-line velocities ($CVEL = 2u(x, 0)$) calculated by Deshpande *et al.* at various Reynolds numbers are reproduced from their figure 11. An ultimate approach to our limiting solution (also shown in figure 10*b*) is certainly not inconsistent with the calculated trends (we note the decrease in $CVEL$ at maximum constriction, and the flattening out beyond, as Re increases), although clearly the Reynolds number effect is still quite pronounced at $Re = 100$. This Re effect is also evident in figure 10(*c*), which compares the solution of Deshpande *et al.* (at $Re = 200$) for the axial velocity profile at maximum constriction (in the model $M0$) with the leading-order theoretical predictions of §§ 4 and 5. The suggested reduction in the velocities there as Re increases is very much in line with the velocity reduction implied in figure 10(*b*).

Qualitatively, all the overall flow patterns calculated by Deshpande *et al.* (e.g. their figure 4*b*), observed or calculated by Lee & Fung (1971) (e.g. their figures 2 and 3) and measured by Young & Tsai also tend to support the present theoretical view (e.g. our figures 1 and 6). However, the Reynolds number effects mentioned above are evident in figures 5(*a*) and (*b*) of Deshpande *et al.*, where the dependence on Re of the major separation position C_2 and of the reattachment position downstream are shown. Clearly the approach to an asymptotic limit is quite slow there, at least as far as C_2 is concerned, although the predictions of §§ 3–5 [that C_2 is given by $x \sim x_{\max} + O(R^{-\frac{1}{16}})$] seem to be in keeping with the variation of C_2. Indeed, bearing in mind the expected $R^{-\frac{1}{16}}$ dependence in (2.1) ff., we feel that the discrepancy between the theory and the calculated or experimental results is satisfactorily small and is due almost entirely to

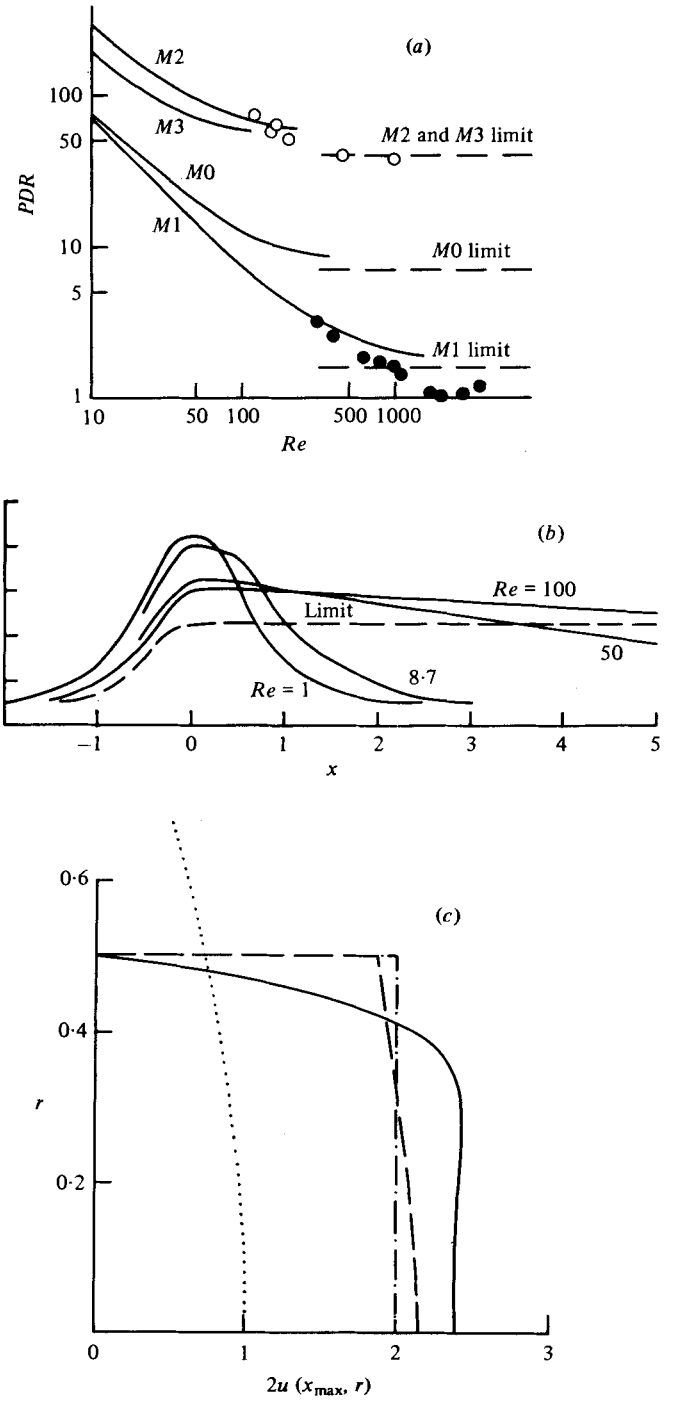

FIGURE 10. (*a*) The pressure drop PDR as a function of Reynolds number Re for the constrictions $M0$, $M1$, $M2$, $M3$ of Deshpande *et al.* (1976). ——, calculations of Deshpande *et al.*; ○, ●, experiments of Young & Tsai (1973); – – –, present theory for slowly varying severe constrictions when $Re \gg 1$. (*b*) Comparisons of the calculated centre-line velocities $CVEL$ of Deshpande *et al.* (solid curves) at various Reynolds numbers and the present (slowly varying) theory for $Re \gg 1$ (dashed curve). (*c*) Comparison of the axial velocity profile at the point of maximum constriction given by Deshpande *et al.* (1976, their figure 10*a*) at $Re = 200$ (solid curve) and by the present theory [– – –, slowly varying (§ 5); — · —, very severe (§ 4)]. The original Poiseuille flow is marked by the dots.

the persisting Reynolds number effects. These effects seem fairly substantial in all of figures 5–8 and 11 of Deshpande *et al.*, and they probably explain also the non-appearance of any upstream separation (at $x = x_{\text{sep}}$) in those constricted flows. Since the prediction of x_{sep} in (2.9) exhibits such a slow growth of $-x_{\text{sep}}$ with the Reynolds number, we might expect the upstream separation to appear only at Reynolds numbers much higher than those of the calculations and experiments above. Alternatively, the upstream separation might appear at the lower Reynolds numbers if the constrictions were more severe or abrupt (as in the asymmetric channel flows of Greenspan 1969; Friedman 1972; Smith 1977*c*, figure 9) than $M0$–$M4$.

Finally, a referee, noting figure 10(*a*) of Deshpande *et al.*, raised the question of concavity in the axial velocity profile through the constriction. Such concavity (i.e. with $u_0(x, r)$ having a local minimum at the centre-line $r = 0$) is indeed possible in the general severe case of § 2, since the very severe case of § 4 always yields concavity at the maximum constriction. For, in general, near $x = x_{\max}$ ($\hat{x} = 0$),

$$\hat{F}_0(\hat{x}) = 1 + \kappa_0 \hat{x}^2 + o(\hat{x}^2),$$

say, from (4.2), where κ_0 (the local curvature) is positive; hence in (4.3),

$$A_0(\hat{x}) \sim \tfrac{1}{4}(1 - 2\kappa_0 \hat{x}^2),$$

while $A_1(\hat{x}) \sim -\frac{1}{8}\kappa_0$ in (4.4*b*). Therefore, at $\hat{x} = 0$, the axial velocity profile is given by

$$u_0 = \tfrac{1}{4}\epsilon^{-2} + \epsilon^{-1}[\tfrac{1}{4}\kappa_0 \hat{r}^2 - \tfrac{1}{8}\kappa_0] + O(1) \qquad \text{(A 1)}$$

from (4.1), (4.3) and (4.4). Thus the theory of § 4 reproduces the concavity exhibited by the solutions of Deshpande *et al.* (given in our figure 10*c*). On the other hand, the moderately severe and slowly varying severe constrictions (§§ 3 and 5) strictly (i.e. for $h \to 0$ or $\lambda \to \infty$) do not allow concavity, because of (3.1) and (5.4*a*) (although if actual values of h or λ are inserted in (3.1) or (5.1) concavity may be implied).

REFERENCES

Batchelor, G. K. 1956 On steady laminar flow with closed streamlines at large Reynolds number. *J. Fluid Mech.* **1**, 177.

Batchelor, G. K. 1967 *An Introduction to Fluid Dynamics*. Cambridge University Press.

Bates, S. 1978 Ph.D. thesis, University of London.

Brodetsky, S. 1923 Discontinuous fluid motion past circular and elliptic cylinders. *Proc. Roy. Soc.* A **102**, 542.

Brown, S. N. & Stewartson, K. 1970 Trailing edge stall. *J. Fluid Mech.* **42**, 561.

Burggraf, O. R. 1970 *U.S. Air Force Aerospace Res. Lab. Rep.* ARL 70-0275.

Burggraf, O. R. 1975 Asymptotic theory of separation and reattachment of a laminar boundary layer on a compression ramp. *AGARD Paper* no. 168.

Deshpande, M. D., Giddens, D. P. & Mabon, F. R. 1976 Steady laminar flow through modelled vascular stenoses. *J. Biomech.* **9**, 165.

Föttinger, H. 1939 *Mitt. Vereinigung Gross-Kesselbesitzer* no. 73, p. 151.

Fraenkel, L. D. 1961 On corner eddies in plane inviscid shear flow. *J. Fluid Mech.* **11**, 400.

Friedman, M. 1972 Laminar flow in a channel with a step. *J. Engng Math.* **6**, 285.

Goldstein, S. 1948 On laminar boundary layer flow near a point of separation. *Quart. J. Mech. Appl. Math.* **1**, 43.

Greenspan, D. 1969 Numerical studies of steady, viscous, incompressible flow in a channel with a step. *J. Engng Math.* **3**, 21.

GROVE, A. S., SHAIR, F. H., PETERSEN, E. E. & ACRIVOS, A. 1964 An experimental investigation of the steady separated flow past a circular cylinder. *J. Fluid Mech.* **19**, 60.

HALL, P. & PARKER, K. H. 1976 The stability of the decaying flow in a suddenly blocked channel. *J. Fluid Mech.* **75**, 305.

HUNG, T.-K. & MACAGNO, E. O. 1966 Laminar eddies in a two-dimensional conduit expansion. *Houille Blanche* **21**, 391.

JENSON, R., BURGGRAF, O. R. & RIZZETTA, D. P. 1974 Asymptotic solution for supersonic viscous flow past a compression corner. *Proc. 4th Int. Conf. Num. Meth. Fluid Mech.*, p. 218. Springer.

JONES, C. W. & WATSON, E. J. 1963 In *Laminar Boundary Layers* (ed. L. Rosenhead), chap. 5. Oxford University Press.

KIRCHHOFF, G. 1869 Zur Theorie freier Flussigkeitsstrahlen. *J. reine angew. Math.* **70**, 289.

LEE, J.-S. & FUNG, J. L. 1970 Flow in locally constricted tubes at low Reynolds numbers. *J. Appl. Mech.* **37**, 9.

LEE, J.-S. & FUNG, J. L. 1971 Flow in non-uniform small blood vessels. *Microvasc. Res.* **3**, 272.

LOCK, R. C. 1951 The velocity distribution in the laminar boundary layer between parallel streams. *Quart. J. Mech.* **4**, 42.

MACAGNO, E. O. & HUNG, T.-K. 1967 Computational and experimental study of a captive annular eddy. *J. Fluid Mech.* **28**, 43.

MELNIK, R. E. & CHOW, R. 1975 Asymptotic theory of two-dimensional trailing edge flows. *Grumman Res. Rep.* RE-510J.

MESSITER, A. F., HOUGH, G. R. & FEO, A. 1973 Base pressure in laminar supersonic flow. *J. Fluid Mech.* **60**, 605.

MILNE-THOMPSON, L. M. 1968 *Theoretical Hydrodynamics*, 5th edn. Macmillan.

ROSHKO, A. 1967 A review of concepts in separated flow. *Proc. Can. Congr. Appl. Mech., Quebec*, vol. 3, p. 81.

SMITH, F. T. 1976*a* Flow through constricted or dilated pipes and channels. *Quart. J. Mech. Appl. Math.* **29**, 343.

SMITH, F. T. 1976*b* Flow through constricted or dilated pipes and channels. Part 2. *Quart. J. Mech. Appl. Math.* **29**, 365.

SMITH, F. T. 1976*c* Pipeflows distorted by nonsymmetric indentation or branching. *Mathematika* **23**, 62.

SMITH, F. T. 1976*d* On entry-flow effects in bifurcating, blocked or constricted tubes. *J. Fluid Mech.* **78**, 709.

SMITH, F. T. 1977*a* Flow through symmetrically constricted tubes. *J. Inst. Math. Appl.* **21**, 145.

SMITH, F. T. 1977*b* The laminar separation of an incompressible fluid streaming past a smooth surface. *Proc. Roy. Soc.* A **356**, 443.

SMITH, F. T. 1977*c* Upstream interactions in channel flows. *J. Fluid Mech.* **79**, 631.

SMITH, F. T. & DUCK, P. W. 1977 Separation of jets or thermal boundary layers from a wall. *Quart. J. Mech. Appl. Math.* **30**, 143.

SOBEY, I. J. 1976 Inviscid secondary motions in a tube of slowly varying ellipticity. *J. Fluid Mech.* **73**, 621.

STEWARTSON, K. 1970*a* Is the singularity at separation removable? *J. Fluid Mech.* **44**, 347.

STEWARTSON, K. 1970*b* On supersonic laminar boundary layers near convex corners. *Proc. Roy. Soc.* A **319**, 289.

STEWARTSON, K. 1974 Multistructured boundary layers on flat plates and related bodies. *Adv. Appl. Mech.* **14**, 145.

STEWARTSON, K. & WILLIAMS, P. G. 1973 Self-induced separation II. *Mathematika* **20**, 98.

SYCHEV, V. YA. 1972 Concerning laminar separation. *Izv. Akad. Nauk SSSR, Mekh. Zh. Gaza* **3**, 47.

TILLETT, J. P. K. 1968 On the laminar flow in a free jet of liquid at high Reynolds number. *J. Fluid Mech.* **32**, 273.

WOODS, L. C. 1955 Two-dimensional flow of a compressible fluid past given curved obstacles with infinite wakes. *Proc. Roy. Soc.* A **227**, 367.

YIH, C.-S. 1959 Two solutions for inviscid rotational flow with corner eddies. *J. Fluid Mech.* **5**, 36.

YIH, C.-S. 1960 Exact solutions for steady two-dimensional flow of a stratified fluid. *J. Fluid Mech.* **9**, 161.

YOUNG, D. F. & TSAI, F. Y. 1973 Flow characteristics in models of arterial stenoses I. Steady flow. *J. Biomech.* **6**, 395.